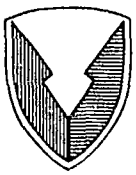

AD

(12)

CONTRACT REPORT BRL-CR-544

A LAGRANGE MULTIPLIER/SEGMENT PROCEDURE FOR SOLUTION OF THREE-DIMENSIONAL CONTACT PROBLEMS

Massachusetts Institute of Technology
Mechanical Engineering Department
Cambridge, MA. 02139

October 1985

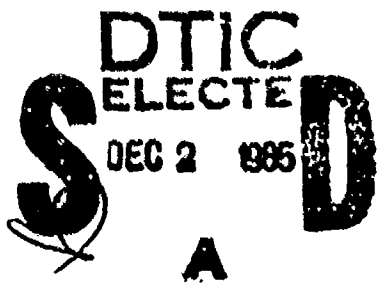

US ARMY BALLISTIC RESEARCH LABORATORY
ABERDEEN PROVING GROUND, MARYLAND

Destroy this report when it is no longer needed.
Do not return it to the originator.

Additional copies of this report may be obtained from the National Technical Information Service, U. S. Department of Commerce, Springfield, Virginia 22161.

The findings in this report are not to be construed as an official Department of the Army position, unless so designated by other authorized documents.

The use of trade names or manufacturers' names in this report does not constitute indorsement of any commercial product.

UNCLASSIFIED
SECURITY CLASSIFICATION OF THIS PAGE (When Data Entered)

REPORT DOCUMENTATION PAGE		READ INSTRUCTIONS BEFORE COMPLETING FORM
1. REPORT NUMBER CONTRACT REPORT BRL-CR-544	2. GOVT ACCESSION NO. AD-A161838	3. RECIPIENT'S CATALOG NUMBER
4. TITLE (and Subtitle) A LAGRANGE MULTIPLIER/SEGMENT PROCEDURE FOR SOLUTION OF THREE DIMENSIONAL CONTACT PROBLEMS		5. TYPE OF REPORT & PERIOD COVERED Contract Report January 1984 to August 1984 6. PERFORMING ORG. REPORT NUMBER
7. AUTHOR(s) A. B. Chaudhary K. J. Bathe		8. CONTRACT OR GRANT NUMBER(s) DAAK11-84-K-0015
9. PERFORMING ORGANIZATION NAME AND ADDRESS Massachusetts Institute of Technology Mechanical Engineering Department; Rm. 3-356 Cambridge, MA. 02139		10. PROGRAM ELEMENT, PROJECT, TASK AREA & WORK UNIT NUMBERS 1L161102AH43
11. CONTROLLING OFFICE NAME AND ADDRESS US Army Ballistic Research Laboratory ATTN: SLCBR-DD-T Aberdeen Proving Ground, MD. 21005-5066		12. REPORT DATE October 1985 13. NUMBER OF PAGES 76
14. MONITORING AGENCY NAME & ADDRESS(if different from Controlling Office)		15. SECURITY CLASS. (of this report) Unclassified 15a. DECLASSIFICATION/DOWNGRADING SCHEDULE

16. DISTRIBUTION STATEMENT (of this Report)

Approved for public release; Distribution unlimited.

17. DISTRIBUTION STATEMENT (of the abstract entered in Block 20, if different from Report)

18. SUPPLEMENTARY NOTES

This work was performed under contract to the Blast Dynamics Branch, Terminal Ballistics Division, US Army Ballistic Research Laboratory, Dr. Joseph M. Santiago, Contracting Officer's Representative.

19. KEY WORDS (Continue on reverse side if necessary and identify by block number)

Contact Problem Algorithm
Finite Element Structural Analysis
Lagrange Multiplier Contact Forces
Multiplier/Segment Procedure
ADINA Finite Element Program
Frictional Sliding and Sticking Contact
Implicit Solution Technique
Hertz axisymmetric contact
Longitudinal Impact of bars

20. ABSTRACT (Continue on reverse side if necessary and identify by block number)

A solution procedure for finite element analysis of three-dimensional contact conditions is presented. The area of contact can vary, frictional conditions are included using Coulomb's law of friction and static or dynamic conditions can be considered. Various sample solutions are presented to demonstrate the applicability of the solution algorithm.

DD FORM 1 JAN 73 1473 EDITION OF 1 NOV 68 IS OBSOLETE

UNCLASSIFIED
SECURITY CLASSIFICATION OF THIS PAGE (When Data Entered)

TABLE OF CONTENTS

TABLE OF CONTENTS (Continued)

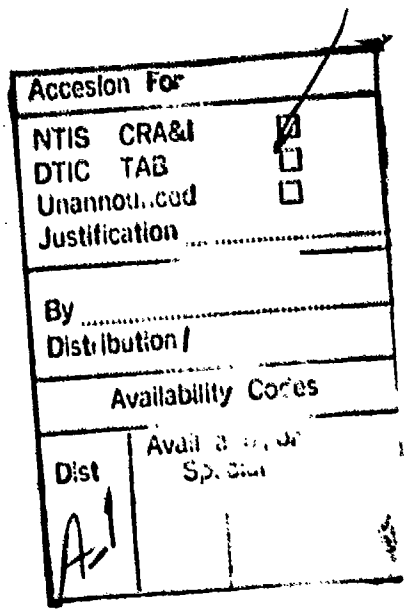

LIST OF FIGURES

LIST OF FIGURES

I. INTRODUCTION

Although much progress has been made during the last decade in the development of computational techniques for nonlinear analysis, there is still a lack of effective solution methods for contact problems. This is largely due to the fact that the analysis of contact problems can be computationally very difficult, even for the simplest geometric conditions and constitutive relations used. Much of the difficulty lies in that the boundary conditions of the bodies under consideration are not known prior to the analysis but depend on the solution variables.

In two earlier communications we presented a solution method for the analysis of general two-dimensional (plane stress, plane strain and axisymmetric) contact conditions [1 2]. The objective of this report is to present an algorithm for three-dimensional contact problems. The solution procedure is an extension of the Lagrange multiplier/segment algorithm, discussed in our earlier work, to three-dimensional analysis and in this report we assume that the reader is familiar with the developments of References [1 2] and the notation of Reference [3].

The Lagrange multiplier/segment algorithm can be employed for three-dimensional large deformation contact problems with variable contact areas, and in static and dynamic conditions. In the following sections we first present the basic equations used in the solution algorithm and discuss the important numerical details. We then give the solution of various example problems to demonstrate the applicability and limitations of the algorithm used. The report concludes with some thoughts on future developments that should be pursued to arrive at improved solution methods for contact problems.

II. SOLUTION METHOD FOR CONTACT - STATICS

The problem considered herein deals with the stress analysis of two bodies, contactor and target, when their boundaries come into contact with each other under the action of external loads (see Fig. 1). The occurrence of contact can be at any arbitrary location on the body boundary and the basic geometric condition of contact is that no material overlap can occur between the bodies. Depending on the external loads, large changes in the region of contact are possible including relative sliding or possible separation after contact. The developed forces of contact on the two bodies must be statically equivalent to each other and for each body the support reactions must be in equilibrium with the externally applied forces and the contact forces.

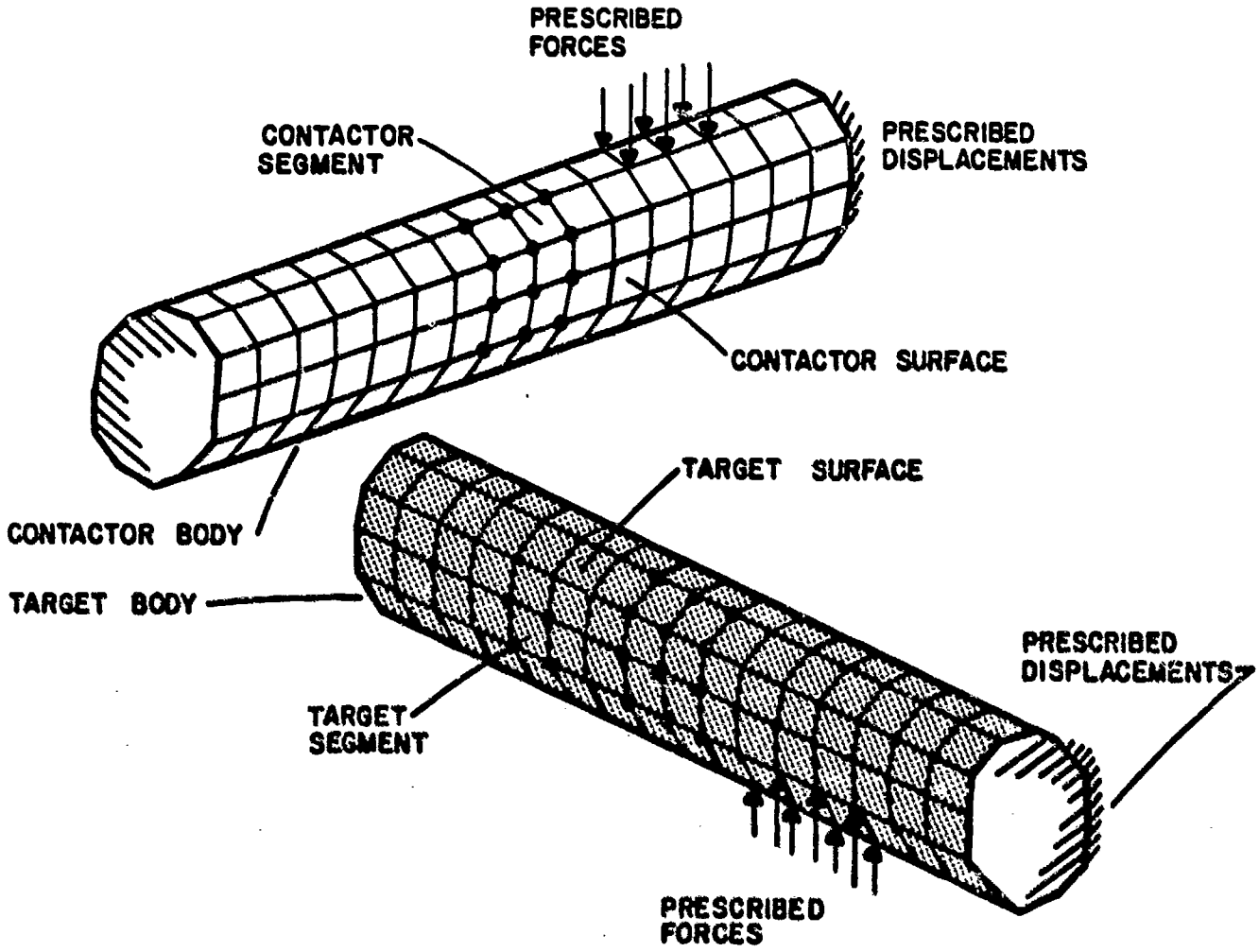

a) Condition prior to contact

Figure 1 Schematic representation of problem considered

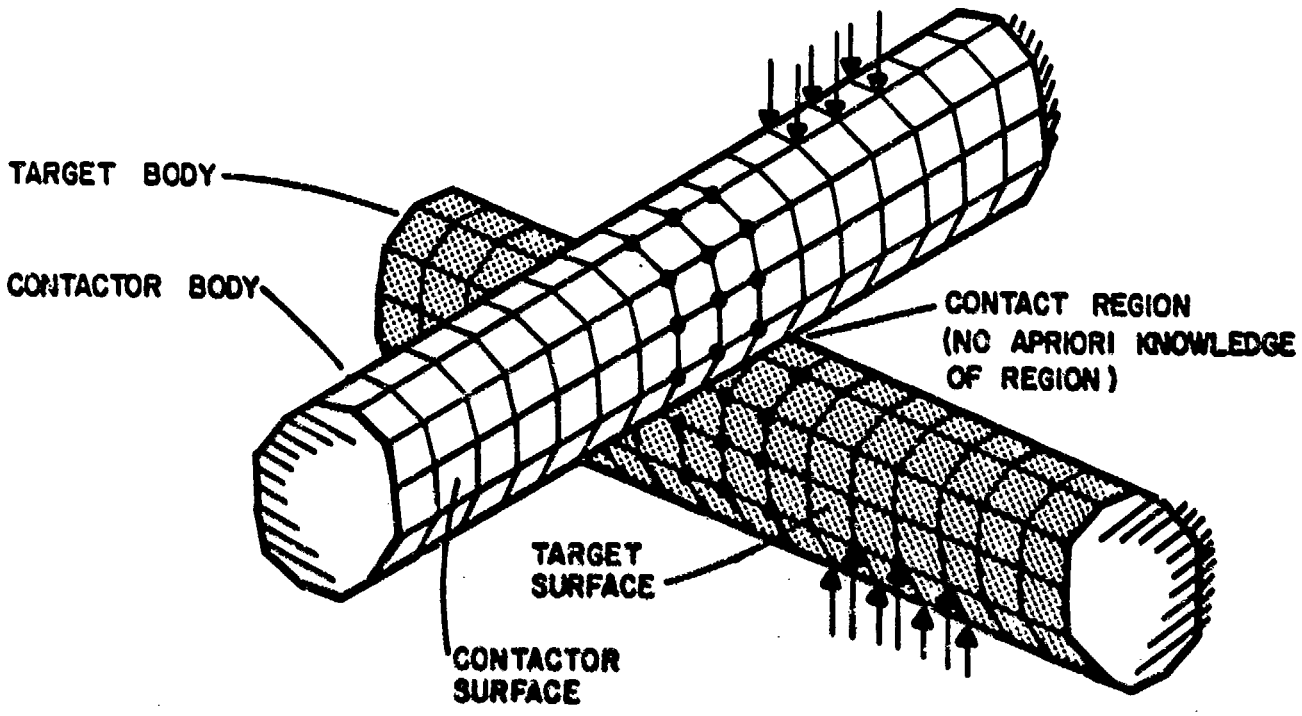

b) Condition at contact

Figure 1 Continued

Although the discussion focuses on two bodies coming into contact with each other, the solution method is also applicable to the analysis of more than two contacting bodies. In that case, one contactor body comes into contact with more than one target body and vice versa. The calculations for contact are performed for each contact region separately and the combined effect onto the incremental equations of equilibrium is obtained by summing the individual contributions by the direct stiffness method.

2.1 Discretization of the Contactor and Target Body Surfaces by Surface Segments

Both the contactor and target surfaces are discretized using four-node quadrilateral segments (see Fig. 1c). Considering the finite elements which are used to discretize the continuum of a body, a generic surface segment corresponds to a finite element face that lies on the body boundary.

In the incremental finite element solution, the contactor surface nodes are considered to come into contact with the target segments. A contactor segment is defined to be in contact if all four nodes belonging to the segment are in cortact with the target surface (see Figs. 1c,d).

In general, the surface segments are non-flat and therefore the following three geometric assumptions are used in the solution procedure:

- For a generic contactor segment, j, the normal vector for the entire segment is approximated by the exact normal to the segment surface at (r=0,s=0), denoted as $\underline{n}_j^C$ (see Fig. 2a). The vector $\underline{n}_j^C$ is used in the calculation of the total normal contact force developed over segment j (see Section 2.5).

- For a generic target segment, j, the normal vector for the entire segment is approximated by the exact normal to the segment surface at (r=0,s=0), denoted as $\underline{n}_j^T$ (see Fig. 2b). The vector $\underline{n}_j^T$ is used in the calculation of constraints on incremental surface displacements due to contact (see Section 2.2).

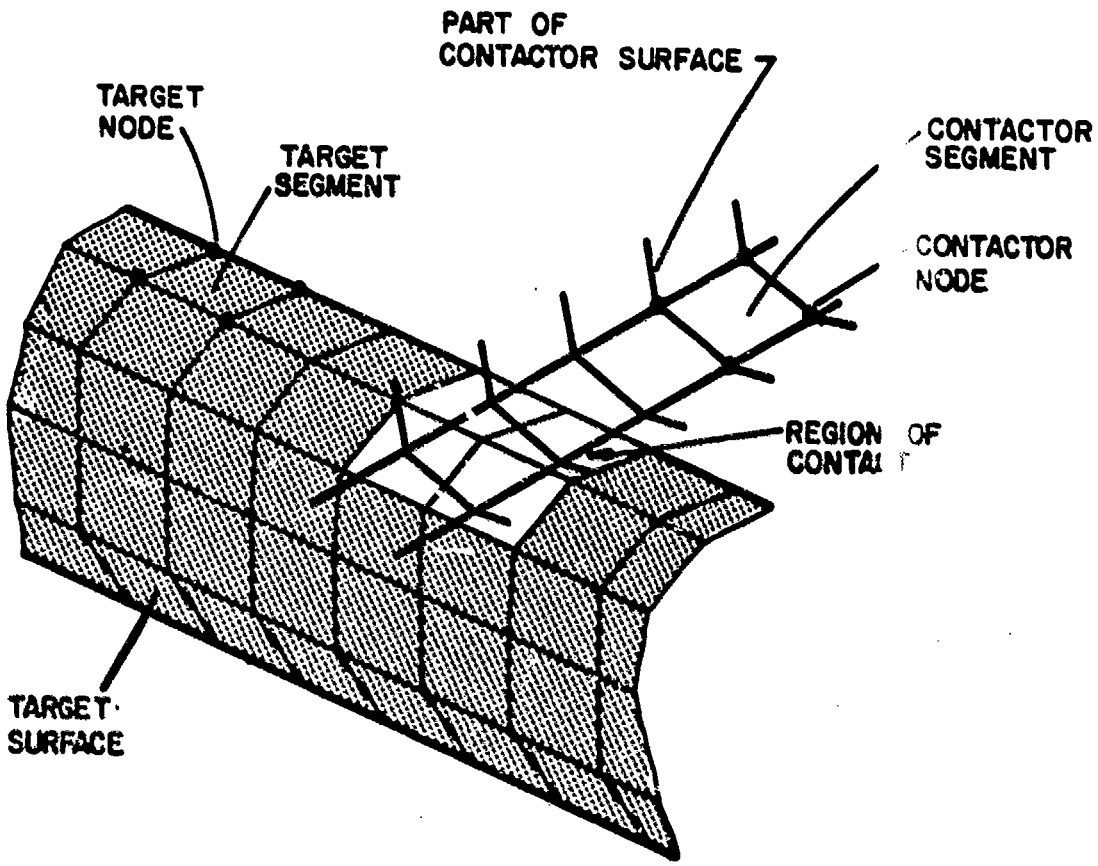

c) Region of contact

Figure 1 Continued

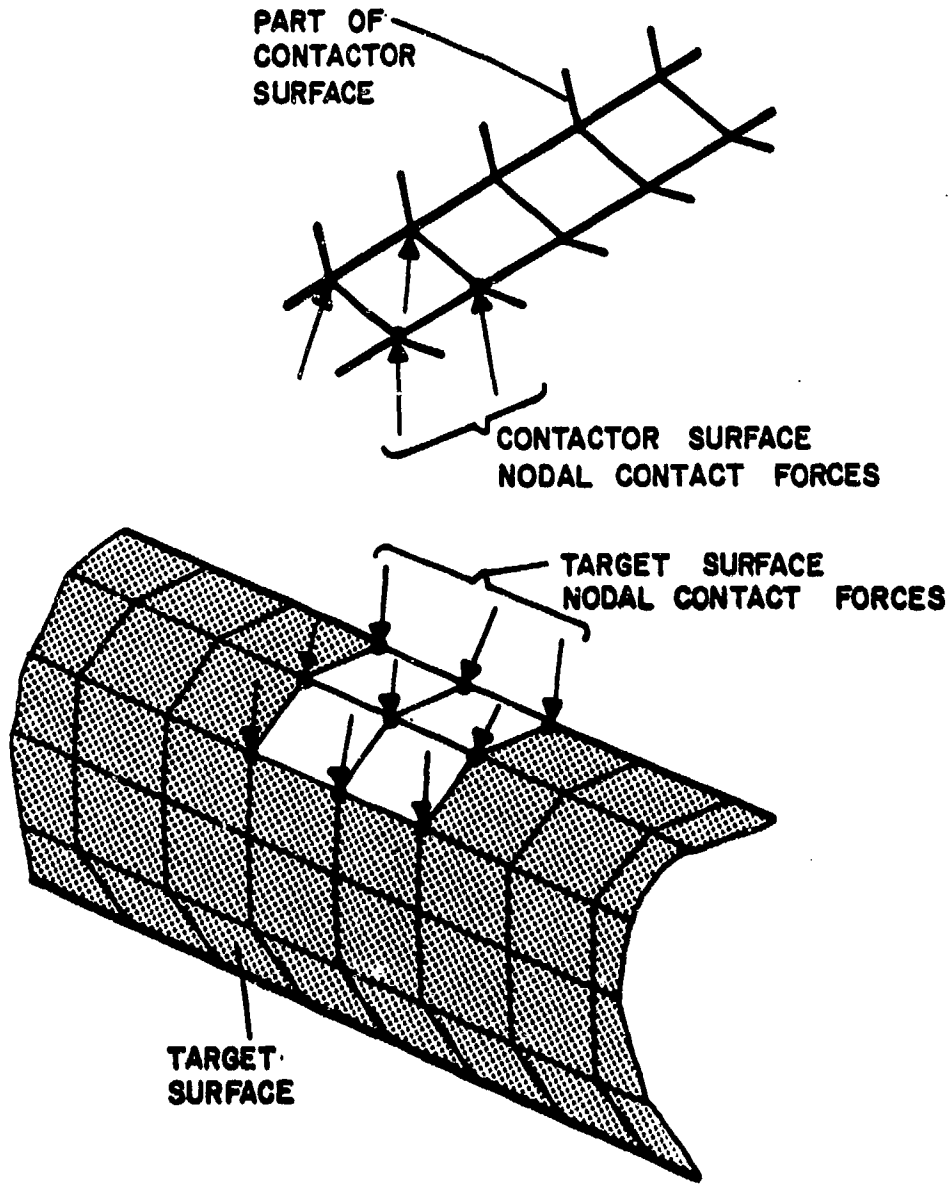

d) Statically equivalent nodal contact forces on the contactor and target surfaces

Figure 1 Continued

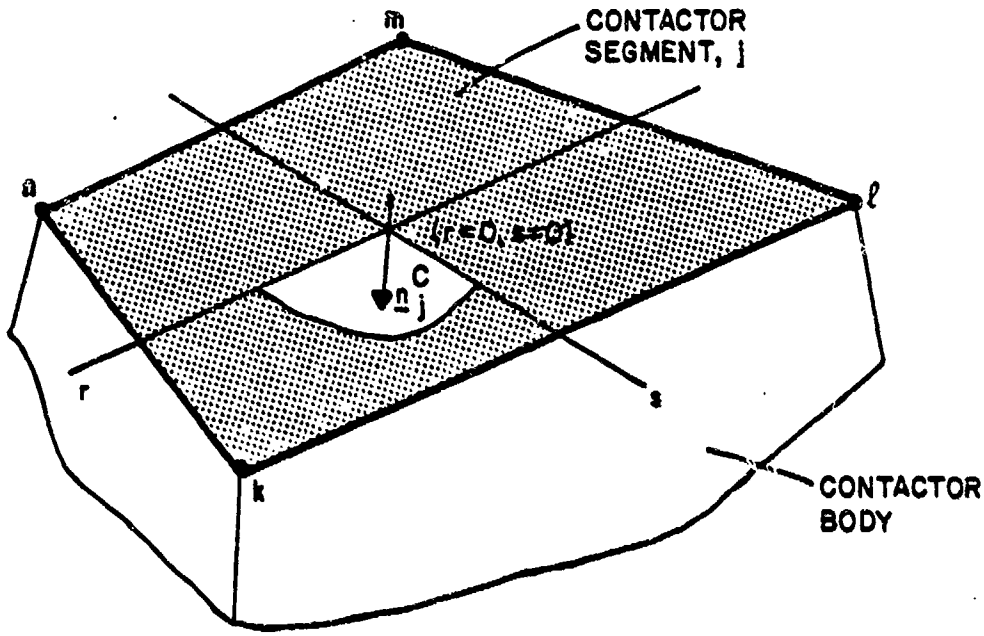

a) Normal vector $\underline{n}_j^C$ to the contactor segment j ($\underline{n}_j^C$ acts into the continuum of the contactor body)

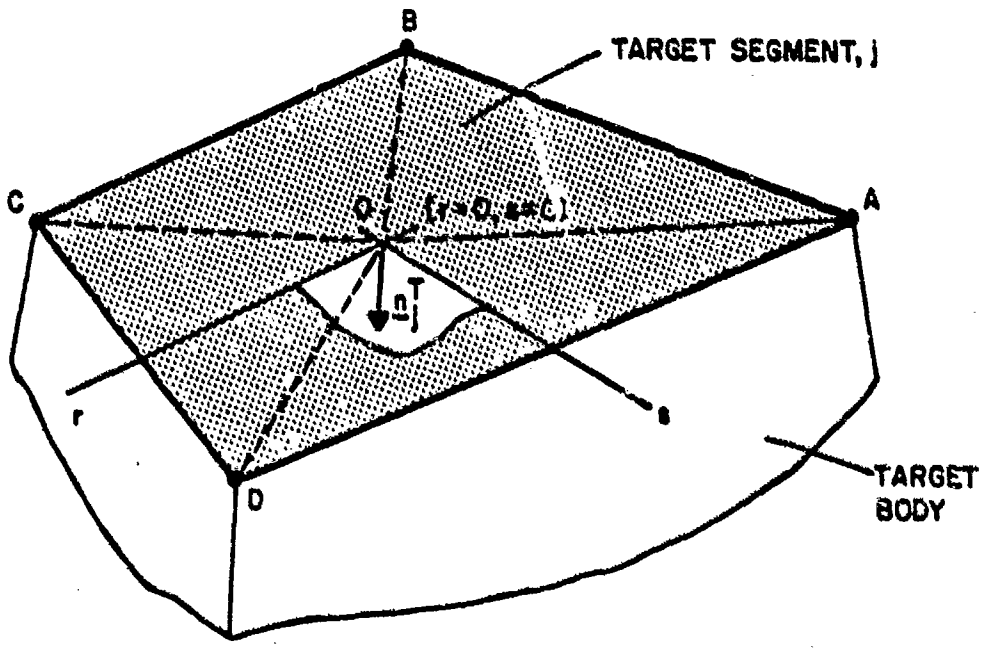

b) Normal vector $\underline{n}_j^T$ to the target segment j ($\underline{n}_j^T$ acts into the continuum of the target body)

Figure 2 Geometry approximations for contactor and target segments

- For a generic target segment, j, the geometry of the segment surface is approximated by four triangles which have one common vertex, 0, (r=0,s=0) (see Figs. 2b,c). Then, considering a generic triangle ABO, the coordinates of any point P within the triangle are given by

$$^{t+\Delta t}\underline{x}_P = \alpha\ ^{t+\Delta t}\underline{x}_A + \beta\ ^{t+\Delta t}\underline{x}_B + \gamma\ ^{t+\Delta t}\underline{x}_O \qquad (1)$$

where,

α,β,γ = triangular area coordinates of point P at time $t+\Delta t$

$^{t+\Delta t}\underline{x}_A$, $^{t+\Delta t}\underline{x}_B$ = global coordinates of target nodes A and B, respectively at time $t+\Delta t$

$^{t+\Delta t}\underline{x}_O$ = global coordinates of vertex 0 (r=0,s=0) at time $t+\Delta t$.

Also, using the bilinear interpolation functions,

$$^{t+\Delta t}\underline{x}_O = \tfrac{1}{4}\left[^{t+\Delta t}\underline{x}_A + {}^{t+\Delta t}\underline{x}_B + {}^{t+\Delta t}\underline{x}_C + {}^{t+\Delta t}\underline{x}_D\right] \qquad (2)$$

where,

$^{t+\Delta t}\underline{x}_C$, $^{t+\Delta t}\underline{x}_D$ = global coordinates of target nodes C and D, respectively at time $t+\Delta t$.

Substituting Eq.(2) into Eq.(1), we obtain

$$^{t+\Delta t}\underline{x}_P = \tfrac{1}{4}\left[(4\alpha+\gamma)^{t+\Delta t}\underline{x}_A + (4\beta+\gamma)^{t+\Delta t}\underline{x}_B + \gamma\,{}^{t+\Delta t}\underline{x}_C + \gamma\,{}^{t+\Delta t}\underline{x}_D\right]. \qquad (3)$$

Equation (3) is used in the calculation of constraints on incremental surface displacements due to contact (see Section 2.2).

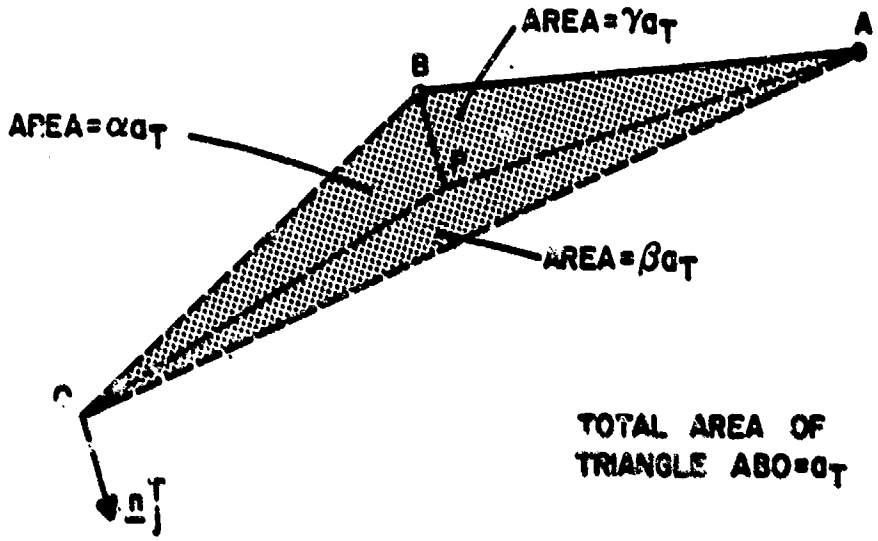

c) Triangle ABO of the target segment j

Figure 2 Continued

2.2 Constraints on Incremental Surface Displacements Due to Contact

After the two bodies have come into contact, the incremental contactor surface displacements must be compatible with the incremental target surface displacements so that the current conditions of sticking contact and sliding contact between the contactor and target surfaces are satisfied. This compatibility of surface displacements is only enforced at the discrete locations corresponding to the contactor nodes. As a result, in an equilibrium configuration, the contactor nodes cannot be within the region of the target body, but the target nodes can be inside or outside the contactor body.

In the iterative solution, the conditions of sticking contact, sliding contact, and tension release at the contactor nodes for the beginning of the next iteration are determined from the contact conditions of the surface segments (see Section 2.6). The necessary geometric constraints to enforce the condition of contact for the incremental displacements at a generic contactor node are discussed in this section. The calculation assumes that the solution response is known at time t and that (i-1) iterations have been performed to calculate the solution at time $t+\Delta t$.

Figure 3 shows how a contactor node k has come into contact with the target segment j formed by nodes A, B, C, and D. Defining point P to be the physical point of contact of node k in the triangle ABO, such that

$$t+\Delta t\underline{x}_P^{(i-1)} = t+\Delta t\underline{x}_k^{(i-1)} - t+\Delta t\underline{\Delta}_k^{(i-1)} \qquad (4)$$

where,

$t+\Delta t\underline{x}_k^{(i-1)}$ = current global coordinates of node k after iteration (i-1) for the equilibrium configuration corresponding to time $t+\Delta t$

$t+\Delta t\underline{\Delta}_k^{(i-1)}$ = material overlap at contactor node k. The calculation of overlap is such that the vectors $t+\Delta t\underline{\Delta}_k^{(i-1)}$ and $\underline{n}_j^T$ are parallel to each other.

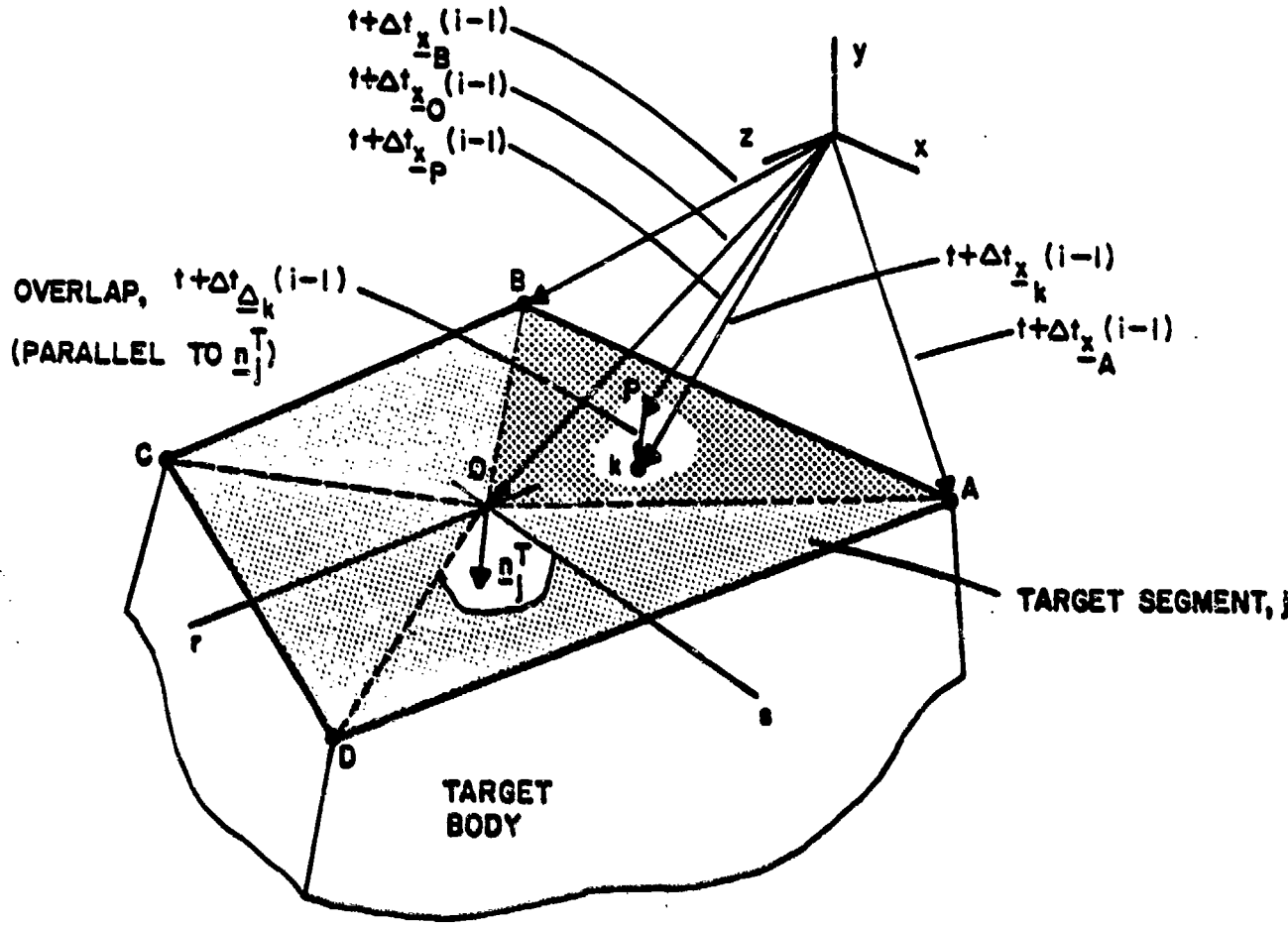

Figure 3 Contactor node k in contact with triangle ABO of target segment j (node k has penetrated into the target body through triangle ABO of target segment j). Note that, in general, the contactor node can come into contact with any of the four triangles of target segment j.

2.2.1 Constraints on Surface Displacements Due to the Condition of Sticking Contact at Node k

For a contactor node k in sticking contact, the incremental displacements in iteration (i) are such that (see Fig. 4)

- the material overlap, $^{t+\Delta t}\underline{\Delta}_k^{(i-1)}$, is eliminated
- the physical point of contact (point P in Fig. 3) with the target segment remains unchanged

Then,

$$^{t+\Delta t}\underline{x}_k^{(i)} = {}^{t+\Delta t}\underline{x}_p^{(i)} \tag{5}$$

Subtracting $^{t+\Delta t}\underline{x}_p^{(i-1)}$ from both sides of Eq. (5),

$$^{t+\Delta t}\underline{x}_k^{(i)} - {}^{t+\Delta t}\underline{x}_p^{(i-1)} = {}^{t+\Delta t}\underline{x}_p^{(i)} - {}^{t+\Delta t}\underline{x}_p^{(i-1)} \tag{6}$$

Substituting Eq. (4) into Eq. (6) and rearranging, we obtain,

$$\Delta\underline{u}_p^{(i)} = \Delta\underline{u}_k^{(i)} + {}^{t+\Delta t}\underline{\Delta}_k^{(i-1)} \tag{7}$$

where,

$\Delta\underline{u}_p^{(i)}$ = incremental displacement of point P in iteration (i)

$\Delta\underline{u}_k^{(i)}$ = incremental displacement of node k in iteration (i).

Using Eq. (3) and assuming an isoparametric interpolation, we hence obtain the following constraint equation,

$$\frac{1}{4}\Big[4(\Delta\underline{u}_k^{(i)} + {}^{t+\Delta t}\underline{\Delta}_k^{(i-1)}) - (4\alpha^{(i-1)} + \gamma^{(i-1)})\Delta\underline{u}_A^{(i)} - (4\beta^{(i-1)} + \gamma^{(i-1)})\Delta\underline{u}_B^{(i)} - \gamma^{(i-1)}\Delta\underline{u}_C^{(i)} - \gamma^{(i-1)}\Delta\underline{u}_D^{(i)}\Big] = 0. \tag{8}$$

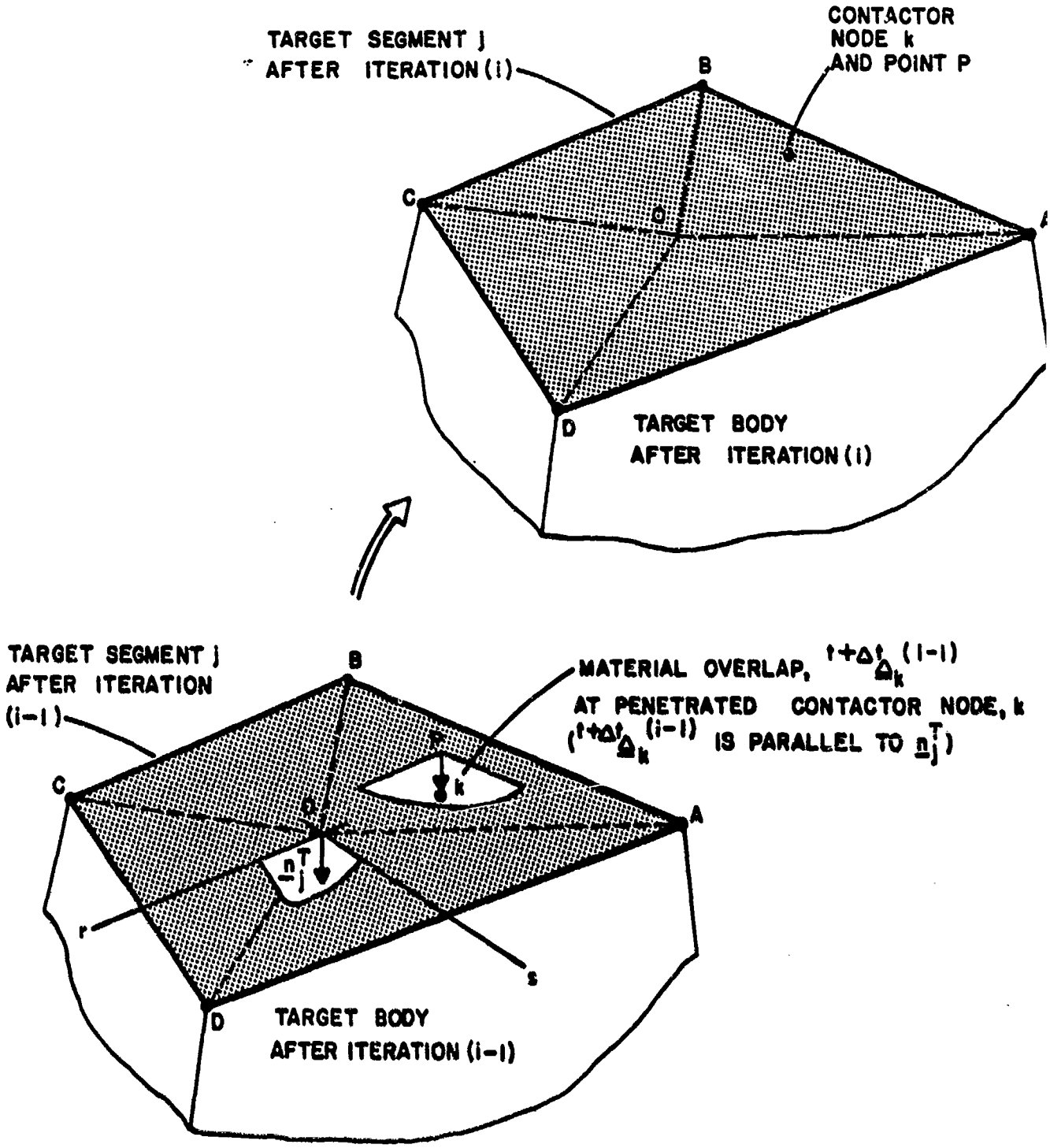

Figure 4 Condition of sticking contact at contactor node k
(also see Fig. 1c)

where,

$\alpha^{(i-1)}$, $\beta^{(i-1)}$, $\gamma^{(i-1)}$ = triangular area coordinates of point P after iteration (i-1)

$\Delta\underline{u}_A^{(i)}$, $\Delta\underline{u}_B^{(i)}$, $\Delta\underline{u}_C^{(i)}$, $\Delta\underline{u}_D^{(i)}$ = incremental displacements at target nodes A, B, C, and D respectively, in iteration (i)

Equation (8) is the constraint of compatible surface displacements for sticking contact between the contactor node k and the target segment j. Equation (8) is used in the calculation of the incremental equations of equilibrium [1].

2.2.2 Constraint on Surface Displacements Due to the Condition of Sliding Contact at Node k

For a contactor node k in sliding contact, the incremental displacements of iteration (i) are such that

- the material overlap, ${}^{t+\Delta t}\underline{\Delta}_k^{(i-1)}$, is eliminated
- the physical point of contact with the target segment can change.

The area coordinates of the physical point of contact after iteration (i) are unknown. So, assuming the amount of sliding in iteration (i) to be small and linearizing about the geometry after iteration (i-1), an approximate constraint of compatible surface displacements for sliding contact is obtained as

$$(\underline{n}_j^T)^T[{}^{t+\Delta t}\underline{x}_p^{(i)} - {}^{t+\Delta t}\underline{x}_p^{(i-1)}] \doteq (\underline{n}_j^T)^T[{}^{t+\Delta t}\underline{x}_k^{(i)} - {}^{t+\Delta t}\underline{x}_p^{(i-1)}] \qquad (9)$$

Substituting Eq. (4) into Eq. (9) and rearranging, we have

$$(\underline{n}_j^T)^T[\Delta\underline{u}_p^{(i)}] \doteq (\underline{n}_j^T)^T[\Delta\underline{u}_k^{(i)} + {}^{t+\Delta t}\underline{\Delta}_k^{(i-1)}] \qquad (10)$$

Using Eq.(3) and assuming an isoparametric interpolation, we hence obtain

$$\frac{1}{2}(\underline{n}_j^T)^T\Big[4(\Delta\underline{u}_k^{(i)} + {}^{t+\Delta t}\underline{\Delta}_k^{(i-1)}) - (4\alpha^{(i-1)} + \gamma^{(i-1)})\Delta\underline{u}_A^{(i)}$$

$$- (4\beta^{(i-1)} + \gamma^{(i-1)})\Delta\underline{u}_B^{(i)} - \gamma^{(i-1)}\Delta\underline{u}_C^{(i)} - \gamma^{(i-1)}\Delta\underline{u}_D^{(i)}\Big] = 0. \quad (11)$$

Equation (11) represents a constraint equation on surface displacements for sliding contact between the contactor node k and the target segment j. Equation (11) is used in the calculation of the incremental equations of equilibrium [1].

2.2.3 Condition of Tension Release at Node k

For a contactor node k which experiences tension release after iteration (i-1), the incremental nodal displacements of iteration (i) are independent of the target segment displacements.

2.3 Incremental Equations of Equilibrium for Contact

The governing equations of motion prior to contact are derived using the procedures described in Reference 3. The solution response of the contactor and target bodies is independent of each other and the unknowns to be calculated in each iteration are the incremental nodal point displacements.

After the occurrence of contact, the effects of constraints on incremental surface displacements (see Eqs. (8) and (11)), are included in the equilibrium equations using a Lagrange multiplier technique [1]. The unknowns to be calculated in each iteration are the incremental nodal point displacements and the incremental contact forces (however, the calculated numerical values of these incremental contact forces are not used subsequently in any contact calculations, see Section 4). The equilibrium equations for iteration (i) at time t+Δt are:

$$\left\{\begin{bmatrix} {}^{t+\Delta t}\underline{K}^{(i-1)} & \underline{0} \\ \underline{0} & \underline{0} \end{bmatrix} + \begin{bmatrix} \underline{0} & {}^{t+\Delta t}\underline{K}_{\lambda}^{(i-1)} \\ {}^{t+\Delta t}\underline{K}_{\lambda}^{(i-1)^T} & \underline{0} \end{bmatrix}\right\} \begin{bmatrix} \Delta\underline{U}^{(i)} \\ \Delta\underline{\lambda}^{(i)} \end{bmatrix}$$

$$= \begin{bmatrix} {}^{t+\Delta t}\underline{R} \\ \underline{0} \end{bmatrix} - \begin{bmatrix} {}^{t+\Delta t}\underline{F}^{(i-1)} \\ \underline{0} \end{bmatrix} + \begin{bmatrix} {}^{t+\Delta t}\underline{R}_C^{(i-1)} \\ {}^{t+\Delta t}\underline{\Delta}_C^{(i-1)} \end{bmatrix} \tag{12}$$

where,

$${}^{t+\Delta t}\underline{K}^{(i-1)} = \begin{bmatrix} {}^{t+\Delta t}\underline{K}_C^{(i-1)} & \underline{0} \\ \underline{0} & {}^{t+\Delta t}\underline{K}_T^{(i-1)} \end{bmatrix} \tag{13}$$

${}^{t+\Delta t}\underline{K}^{(i-1)}$ = Usual tangent stiffness matrix including material and geometric nonlinearities after iteration (i-1)

${}^{t+\Delta t}\underline{K}_C^{(i-1)}$ = Usual tangent stiffness matrix for the contactor body after iteration (i-1)

${}^{t+\Delta t}\underline{K}_T^{(i-1)}$ = Usual tangent stiffness matrix for the target body after iteration (i-1)

${}^{t+\Delta t}\underline{K}_{\lambda}^{(i-1)}$ = Contact matrix to include the constraints of compatible surface displacements after iteration (i-1) (see Section 2.2)

${}^{t+\Delta t}\underline{R}$ = Vector of total applied external forces at time t+Δt

$^{t+\Delta t}\underline{F}^{(i-1)}$ = Vector of nodal point forces equivalent to element stresses after iteration (i-1)

$^{t+\Delta t}\underline{R}_c^{(i-1)}$ = Vector of updated contact forces after iteration (i-1) (see Section 2.5)

$^{t+\Delta t}\underline{\Delta}_c^{(i-1)}$ = Vector of material overlaps at contactor nodes after iteration (i-1) (see Section 2.2)

$\Delta\underline{U}^{(i)}$ = Vector of incremental nodal point displacements in iteration (i)

$\Delta\underline{\lambda}^{(i)}$ = Vector of increments in contact forces in iteration (i) (see Section 4).

In Eq. (12), the second row corresponds to the constraints on incremental surface displacements due to contact. The increments in contact forces, $\Delta\underline{\lambda}^{(i)}$, enforce the constraints of contact for iteration (i) (i.e., $\Delta\underline{\lambda}^{(i)}$ are Lagrange multipliers).

All surface nodes which belong to the contact region contribute to the contact matrices, $^{t+\Delta t}\underline{K}_\lambda^{(i-1)}$, $^{t+\Delta t}\underline{R}_c^{(i-1)}$, and $^{t+\Delta t}\underline{\Delta}_c^{(i-1)}$. The sum total effect of all surface nodes on the contact matrices is obtained by summing the individual contributions using the direct stiffness method.

The calculation of $^{t+\Delta t}\underline{K}^{(i-1)}$, $^{t+\Delta t}\underline{R}$, and $^{t+\Delta t}\underline{F}^{(i-1)}$ is performed using the usual procedures (see Reference 3).

2.4 Contact Matrices for Sticking Contact and Sliding Contact

In this section, the matrices $^{t+\Delta t}\underline{K}_\lambda^{(i-1)}$, $^{t+\Delta t}\underline{R}_c^{(i-1)}$, and $^{t+\Delta t}\underline{\Delta}_c^{(i-1)}$ are given for a generic region of contact consisting of the contactor node k and its target segment of contact j (see Fig. 3).

2.4.1 Condition of Sticking Contact

The matrices for sticking contact are:

$$\underset{(15 \times 3)}{{}^{t+\Delta t}\underline{K}_{\lambda}^{(i-1)}} = \begin{bmatrix} & & -\underline{I} \\ \tfrac{1}{4}(4\alpha^{(i-1)} + \gamma^{(i-1)}) & & \underline{I} \\ \tfrac{1}{4}(4\beta^{(i-1)} + \gamma^{(i-1)}) & & \underline{I} \\ & \tfrac{1}{4}\gamma^{(i-1)} & \underline{I} \\ & \tfrac{1}{4}\gamma^{(i-1)} & \underline{I} \end{bmatrix} \tag{14}$$

$$\underset{(15 \times 1)}{{}^{t+\Delta t}\underline{R}_{C}^{(i-1)}} = \begin{bmatrix} {}^{t+\Delta t}\underline{\lambda}_{k}^{(i-1)} \\ -\tfrac{1}{4}(4\alpha^{(i-1)} + \gamma^{(i-1)})\ {}^{t+\Delta t}\underline{\lambda}_{k}^{(i-1)} \\ -\tfrac{1}{4}(4\beta^{(i-1)} + \gamma^{(i-1)})\ {}^{t+\Delta t}\underline{\lambda}_{k}^{(i-1)} \\ -\tfrac{1}{4}\gamma^{(i-1)}\ {}^{t+\Delta t}\underline{\lambda}_{k}^{(i-1)} \\ -\tfrac{1}{4}\gamma^{(i-1)}\ {}^{t+\Delta t}\underline{\lambda}_{k}^{(i-1)} \end{bmatrix} \tag{15}$$

$$\underset{(3 \times 1)}{{}^{t+\Delta t}\underline{\Delta}_c^{(i-1)}} = \left[{}^{t+\Delta t}\underline{\Delta}_k^{(i-1)} \right] \tag{16}$$

where,

$$\underline{I} = \begin{bmatrix} 1 & 0 & 0 \\ 0 & 1 & 0 \\ 0 & 0 & 1 \end{bmatrix} \tag{17}$$

$$= \text{identity matrix; } (3 \times 3)$$

${}^{t+\Delta t}\underline{\lambda}_k^{(i-1)}$ = Contact force at contactor node k after iteration (i-1) corresponding to the x, y, and z coordinate axes (see Section 2.5).

Also, the solution vector for iteration (i) is

$$\underset{(18 \times 1)}{\begin{bmatrix} \Delta\underline{U}^{(i)} \\ \Delta\underline{\lambda}^{(i)} \end{bmatrix}} = \begin{bmatrix} \Delta\underline{u}_k^{(i)} \\ \Delta\underline{u}_A^{(i)} \\ \Delta\underline{u}_B^{(i)} \\ \Delta\underline{u}_C^{(i)} \\ \Delta\underline{u}_D^{(i)} \\ \Delta\underline{\lambda}_k^{(i)} \end{bmatrix} \tag{18}$$

where $\Delta\underline{\lambda}_k^{(i)}$ is the vector of increments in the contact force at contactor node k in iteration (i).

Note that by substituting Eqs. (14), (16), and (18) into Eq. (12) the constraint of compatible surface displacements for sticking contact is generated (see Eq. (8)). Thus, to enforce sticking contact, three individual equations are necessary to constrain the x,y, and z incremental displacements of node k to the x,y, and z incremental displacements of point P respectively (see Fig. 4).

2.4.2 Condition of Sliding Contact

The matrices for sliding contact are:

$$
{}^{t+\Delta t}\underset{(15 \times 1)}{\underline{K}_{\lambda}}{}^{(i-1)} = \begin{bmatrix} & & -\underline{n}_j^T \\ & & \\ & & \tfrac{1}{4}\left(4\alpha^{(i-1)} + \gamma^{(i-1)}\right)\ \underline{n}_j^T \\ & & \tfrac{1}{4}\left(4\beta^{(i-1)} + \gamma^{(i-1)}\right)\ \underline{n}_j^T \\ & & \\ & \tfrac{1}{4}\gamma^{(i-1)}\ \underline{n}_j^T & \\ & & \\ & \tfrac{1}{4}\gamma^{(i-1)}\ \underline{n}_j^T & \end{bmatrix} \qquad (19)
$$

$$
{}^{t+\Delta t}\underset{(1 \times 1)}{\underline{\Delta}_c}{}^{(i-1)} = \left[\left(\underline{n}_j^T\right)^T \quad {}^{t+\Delta t}\underline{\Delta}_k{}^{(i-1)} \right]. \qquad (20)
$$

The vector ${}^{t+\Delta t}\underline{R}_c{}^{(i-1)}$ for sliding contact is as given in Eq. (15). The solution vector for iteration (i) is

$$\underset{(16 \times 1)}{\begin{bmatrix} \Delta \underline{U}^{(i)} \\ \Delta \underline{\lambda}^{(i)} \end{bmatrix}} = \begin{bmatrix} \Delta \underline{u}_k^{(i)} \\ \Delta \underline{u}_A^{(i)} \\ \Delta \underline{u}_B^{(i)} \\ \Delta \underline{u}_C^{(i)} \\ \Delta \underline{u}_D^{(i)} \\ \Delta \lambda_k^{(i)} \end{bmatrix} \tag{21}$$

where $\Delta\lambda_k^{(i)}$ is the increment in the normal contact force at contactor node k in iteration (i). Or,

$$\Delta \underline{\lambda}_k^{(i)} = \Delta\lambda_k^{(i)} \, \underline{n}_j^T \tag{22}$$

Note that by substituting Eqs. (19), (20) and (21) into Eq. (12), the constraint of compatible surface displacements for sliding contact is generated (see Eq. (11)). Thus, to enforce sliding contact, one equation is necessary to constrain the incremental displacement of node k along the direction $\underline{n}_j^T$ to the incremental displacement of point P along the same direction $\underline{n}_j^T$ (see Section 2.2).

2.5 Evaluation of the Contact Forces After Iteration (i-1)

After each iteration, the generated contact forces at the contactor nodes are updated such that Coulomb's law of friction is enforced in a global sense over each contactor segment [1 2]. The contact forces at the target nodes are updated such that they are statically equivalent to the updated forces at the contactor nodes. The updated nodal contact forces are the elements of the vector $^{t+\Delta t}\underline{R}_C^{(i-1)}$ (see Eq. (15)).

For a generic contactor node k which belongs to the region of contact, the contact nodal point force vector prior to updating, $\Delta \underline{R}_k^{(i-1)}$, is obtained as

$$\Delta \underline{R}_k^{(i-1)} = {}^{t+\Delta t}\underline{F}_k^{(i-1)} - {}^{t+\Delta t}\underline{R}_k \tag{23}$$

where ${}^{t+\Delta t}\underline{F}_k^{(i-1)}$ and ${}^{t+\Delta t}\underline{R}_k$ are the elements of vectors ${}^{t+\Delta t}\underline{F}^{(i-1)}$ and ${}^{t+\Delta t}\underline{R}$ corresponding to the degrees of freedom of node k respectively. Considering all contactor nodes belonging to the contact region, the vector of nodal point contact forces prior to updating is denoted as $\Delta \underline{R}^{(i-1)}$ and the elements of $\Delta \underline{R}^{(i-1)}$ corresponding to node k are denoted as $\Delta \underline{R}_k^{(i-1)}$.

Physically, $\Delta \underline{R}_k^{(i-1)}$ is (minus) the out-of-balance force vector usually encountered in nonlinear analyses without contact conditions. In the presence of contact, when convergence is reached after iteration (i-1), $\Delta \underline{R}_k^{(i-1)}$ is equal to the contact nodal point force vector at node k (see Fig. 1d).

The updated contact forces after iteration (i-1), ${}^{t+\Delta t}\underline{R}_c^{(i-1)}$, are calculated from the contactor surface nodal forces, $\Delta \underline{R}^{(i-1)}$, in the following three steps:

- Distributed segment tractions are recovered on the contactor surface such that they are equivalent (in the virtual work sense) to the nodal contact forces, $\Delta \underline{R}^{(i-1)}$.

- The distributed contactor segment tractions are updated to satisfy Coulomb's law of friction. The updated contactor surface nodal forces are obtained as the consistent nodal loads corresponding to the updated segment tractions.

- The target surface updated nodal contact forces are obtained from the contactor surface updated nodal forces by considering static equilibrium of the contact region after iteration (i-1) (see Fig. 3 and Eq. (15)).

2.5.1 Recovery of Segment Tractions on the Contactor Surface

The segment traction recovery calculation uses the following two assumptions:

- The interpolation of tractions over each contactor segment is bilinear.
- The tractions are continuous across the segment boundaries.

Figure 5 shows the distribution of segment tractions over a generic contactor segment j. The consistent nodal loads corresponding to the distributed segment tractions are given by

$$\underline{\Delta R}_j = \underline{G}\,\underline{t}_j \tag{24}$$

where,

$$\underline{t}_j = \begin{bmatrix} t_x^k & t_y^k & t_z^k \\ t_x^\ell & t_y^\ell & t_z^\ell \\ t_x^m & t_y^m & t_z^m \\ t_x^n & t_y^n & t_z^n \end{bmatrix} \tag{25}$$

= nodal point values of the segment tractions (e.g. t_x^k is the x-component of the segment traction at node k)

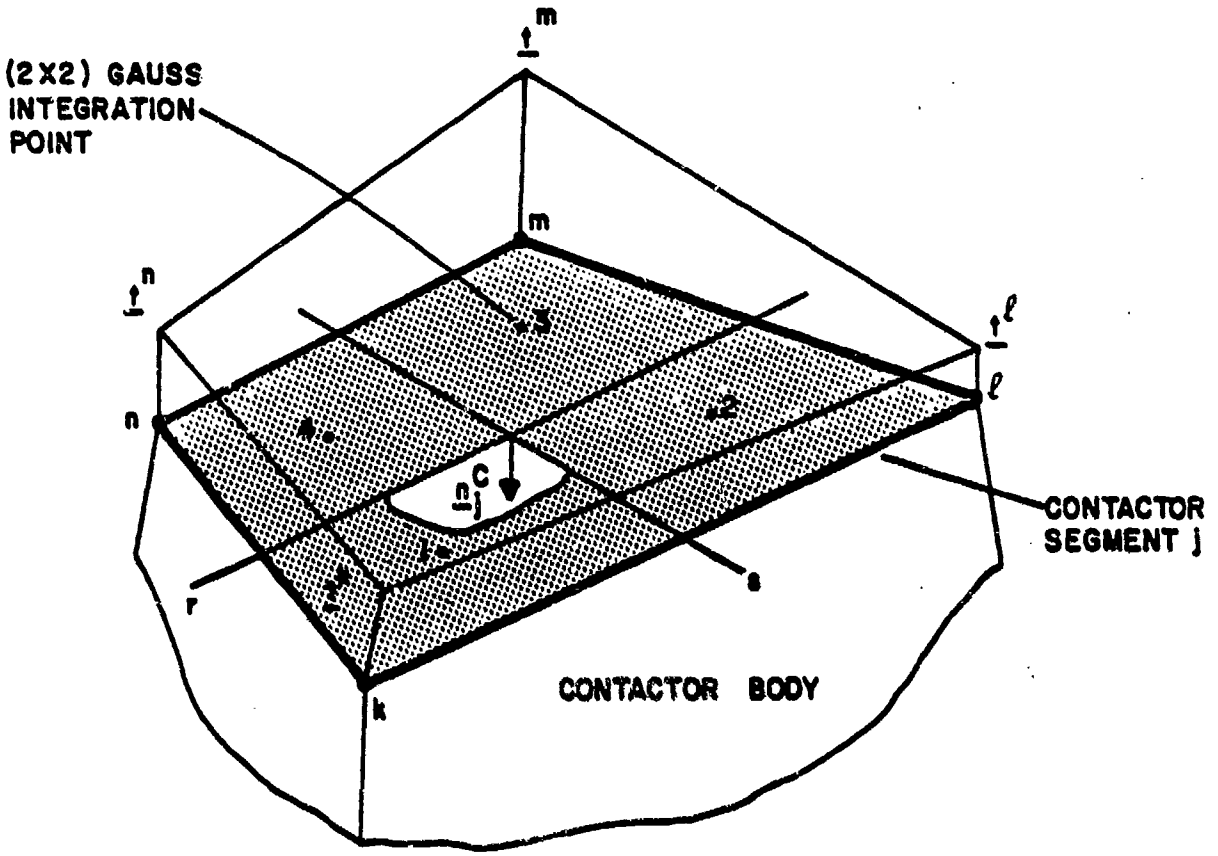

Figure 5 Contactor segment traction distribution ($\underline{t}^k$, $\underline{t}^\ell$, $\underline{t}^m$, and $\underline{t}^n$ are the values of segment tractions at segment nodal points k, ℓ, m, and n respectively)

$$\Delta\underline{R}_j = \begin{bmatrix} \Delta R_x^k & \Delta R_y^k & \Delta R_z^k \\ \Delta R_x^\ell & \Delta R_y^\ell & \Delta R_z^\ell \\ \Delta R_x^m & \Delta R_y^m & \Delta R_z^m \\ \Delta R_x^n & \Delta R_y^n & \Delta R_z^n \end{bmatrix} \tag{26}$$

= consistent nodal point forces corresponding to the segment tractions (e.g., ΔR_x^k is the x-component of the consistent nodal load at node k due to the distributed segment tractions over segment j only. The total force $\Delta\underline{R}_k^{(i-1)}$ at node k is the sum of contributions from the tractions acting over all segments adjoining node k).

$\underline{G}$ = coefficient matrix relating nodal values of segment tractions to the corresponding consistent nodal loads.

The matrix $\underline{G}$ is evaluated by (2 x $\bar{2}$) numerical integration [3] as

$$\underline{G} = \underline{\bar{H}}^T \underline{J} \underline{\bar{H}} \tag{27}$$

where,

$$\underline{\bar{H}} = \begin{bmatrix} \bar{h}_{11} & \bar{h}_{12} & \bar{h}_{13} & \bar{h}_{14} \\ & \bar{h}_{22} & \bar{h}_{23} & \bar{h}_{24} \\ & & \bar{h}_{33} & \bar{h}_{34} \\ \text{symmetric} & & & \bar{h}_{44} \end{bmatrix} \tag{28}$$

= matrix of values of the bilinear interpolation functions at the (2 x 2) Gauss integration points

$$\underline{J} = \begin{bmatrix} J_1 & & & \\ & J_2 & & \\ & & J_3 & \\ & & & J_4 \end{bmatrix} \tag{29}$$

= diagonal matrix of values of the Jacobian determinant at the (2 x 2) Gauss integration points

$$\bar{h}_{11} = \bar{h}_{22} = \bar{h}_{33} = \bar{h}_{44} = 0.62200847$$
$$\bar{h}_{12} = \bar{h}_{23} = \bar{h}_{34} = \bar{h}_{14} = 0.16666666$$
$$\bar{h}_{13} = \bar{h}_{24} = 0.04465820$$

Using Eq. (24) and summing the contributions from all contactor segments belonging to the contact region, a coefficient matrix relating the nodal values of segment tractions to the nodal contact forces (i.e., the contact forces given by Eq. (23)) is constructed. A Gauss elimination solution is subsequently performed to obtain the unknown nodal values of the segment tractions.

2.5.2 Friction Update of Segment Tractions

Using the recovered segment tractions, the total segment contact force, $\underline{T}^j$, is obtained from Eq. (24) as:

$$\underline{T}^j = [\ \underline{G}_T\ \underline{t}_j\ ]^T \tag{30}$$

where

$$\left[\underline{G}_T\right]^T = \begin{bmatrix} \bar{h}_{11}J_1 + \bar{h}_{12}J_2 + \bar{h}_{13}J_3 + \bar{h}_{14}J_4 \\ \bar{h}_{12}J_1 + \bar{h}_{22}J_2 + \bar{h}_{23}J_3 + \bar{h}_{24}J_4 \\ \bar{h}_{13}J_1 + \bar{h}_{23}J_2 + \bar{h}_{33}J_3 + \bar{h}_{34}J_4 \\ \bar{h}_{14}J_1 + \bar{h}_{24}J_2 + \bar{h}_{34}J_3 + \bar{h}_{44}J_4 \end{bmatrix} \tag{31}$$

Also,

$$\underline{T}_n^j = [(\underline{T}^j)^T \underline{n}_j^C] \underline{n}_j^C \tag{32}$$

$$\underline{T}_t^j = \underline{T}^j - \underline{T}_n^j \tag{33}$$

where $\underline{T}_n^j$ and $\underline{T}_t^j$ are the total normal and tangential segment contact forces respectively.

Using $\underline{T}_n^j$ and $\underline{T}_t^j$, the procedure for updating the segment tractions to enforce Coulomb's law of friction is as follows:

- Condition of Tension Release

  A contactor segment experiences tension release after iteration (i-1) if the total normal segment contact force is tensile.
  Since the segment normal vector $\underline{n}_j^C$ points into the continuum of the contactor body (see Fig. 2), a tensile normal segment force acts in the opposite direction of $\underline{n}_j^C$. Thus, segment tension release is detected if

$$(\underline{T}^j)^T \underline{n}_j^C < 0 . \tag{34}$$

  The segment tractions are updated to zero. Hence

$$\hat{\underline{t}}_j = \underline{0} \tag{35}$$

$$\underline{\Lambda}_j = \underline{0} \tag{36}$$

  where

  $\hat{\underline{t}}_j$ = matrix of updated nodal point values of segment tractions.

  $\underline{\Lambda}_j$ = matrix of consistent segment nodal point forces corresponding to the updated tractions over segment j.

- Condition of Sliding Contact

A contactor segment experiences sliding contact after iteration (i-1) if the total segment tangential force exceeds the total segment frictional capacity, or

$$T_t^j > T_f^j \tag{37}$$

where

$$T_t^j = \left| \underline{T}_t^j \right| \tag{38}$$

$$T_f^j = \mu \left[(\underline{T}^j)^T \underline{n}_j C \right] \tag{39}$$

T_f^j = total segment frictional capacity

μ = coefficient of friction

The tangential component of the segment tractions is updated to be a constant value $\hat{\underline{t}}_t$ for the entire segment j such that [1],

$$\hat{\underline{t}}_t = \left[\frac{T_f^j}{T_t^j} \right] \frac{\underline{T}_t^j}{A_j} \tag{40}$$

where

$$A_j = J_1 + J_2 + J_3 + J_4 \tag{41}$$

A_j = area of segment j

And also

$$\hat{\underline{t}}_j = \underline{t}_n^j + \hat{\underline{t}}_t^j \tag{42}$$

$$\underline{\Lambda}_j = \underline{G}\, \hat{\underline{t}}_j \tag{43}$$

where

$$\underline{t}_n^j = [\underline{t}_j \ \underline{n}_j^C] \ [\underline{n}_j^C]^T \tag{44}$$

= nodal point values of the normal component of the recovered segment tractions

$$\underline{\hat{t}}_t^j = [\ \underline{\hat{t}}_t \quad \underline{\hat{t}}_t \quad \underline{\hat{t}}_t \quad \underline{\hat{t}}_t\ ]^T \tag{45}$$

= nodal point values of the updated tangential segment traction (see Eq. (40)).

Note that using Eq. (40), the magnitude of the total tangential segment force is scaled down to equal the segment frictional capacity. The direction of the updated tangential force is as for the force $\underline{T}_t^j$. However, the direction of the actual relative sliding of the contactor segment j (with respect to the target surface) in iteration (i) is not enforced to be opposite to the direction of the updated tangential force (see Eqs. (12) and (19)).

For the condition of contact with no friction, all contactor segments which do not experience tension release are in sliding contact.

- Condition of Sticking Contact

A contactor segment experiences sticking contact after iteration (i-1) if the total segment tangential force is less than (or equal to) the total segment frictional capacity, or

$$T_t^j \leq T_f^j . \tag{46}$$

The segment tractions satisfy Coulomb's law of friction and thus

$$\underline{\hat{t}}_j = \underline{t}_j \tag{47}$$

$$\underline{\Lambda}_j = \underline{\Delta R}_j . \tag{48}$$

For the condition of contact with infinite friction, all contactor segments which do not experience tension release are in sticking contact.

By summing the updated segment nodal forces, the total updated contact forces at the contactor nodes are obtained. For a contactor node k, the updated force is denoted as $^{t+\Delta t}\underline{\lambda}_k^{(i-1)}$ (see Eq. (15)).

In general, the contact region comprises a number of contactor segments and solitary contactor nodes (see Fig. 6). A contactor node k is denoted as a solitary node in contact if

- The node k is in contact
- None of the adjoining contactor segments to node k are in contact. This condition occurs if for each of the adjoining segments, the number of segment nodes in contact is less than four (see Section 2.1).

The update of the contact force at a generic solitary node in contact, k, is performed as follows:

- Obtain the contact force $\Delta\underline{R}_k^{(i-1)}$ at the solitary node (see Eq. (23)).
- At the solitary node, evaluate the normal vector to the contactor surface, $\underline{n}_k^C$, as the average of the normal vectors of the adjoining surface segments.
- Calculate the normal contact force, $\underline{T}_n^k$, and the tangential contact force, $\underline{T}_t^k$, as

$$\underline{T}_n^k = [(\Delta\underline{R}_k^{(i-1)})^T \underline{n}_k^C] \underline{n}_k^C \tag{49}$$

$$\underline{T}_t^k = \Delta\underline{R}_k^{(i-1)} - \underline{T}_n^k \tag{50}$$

- Evaluate the updated contact force at node k in analogy to the evaluation for a contact segment:

For tension release

$$^{t+\Delta t}\underline{\lambda}_k^{(i-1)} = \underline{0} \tag{51}$$

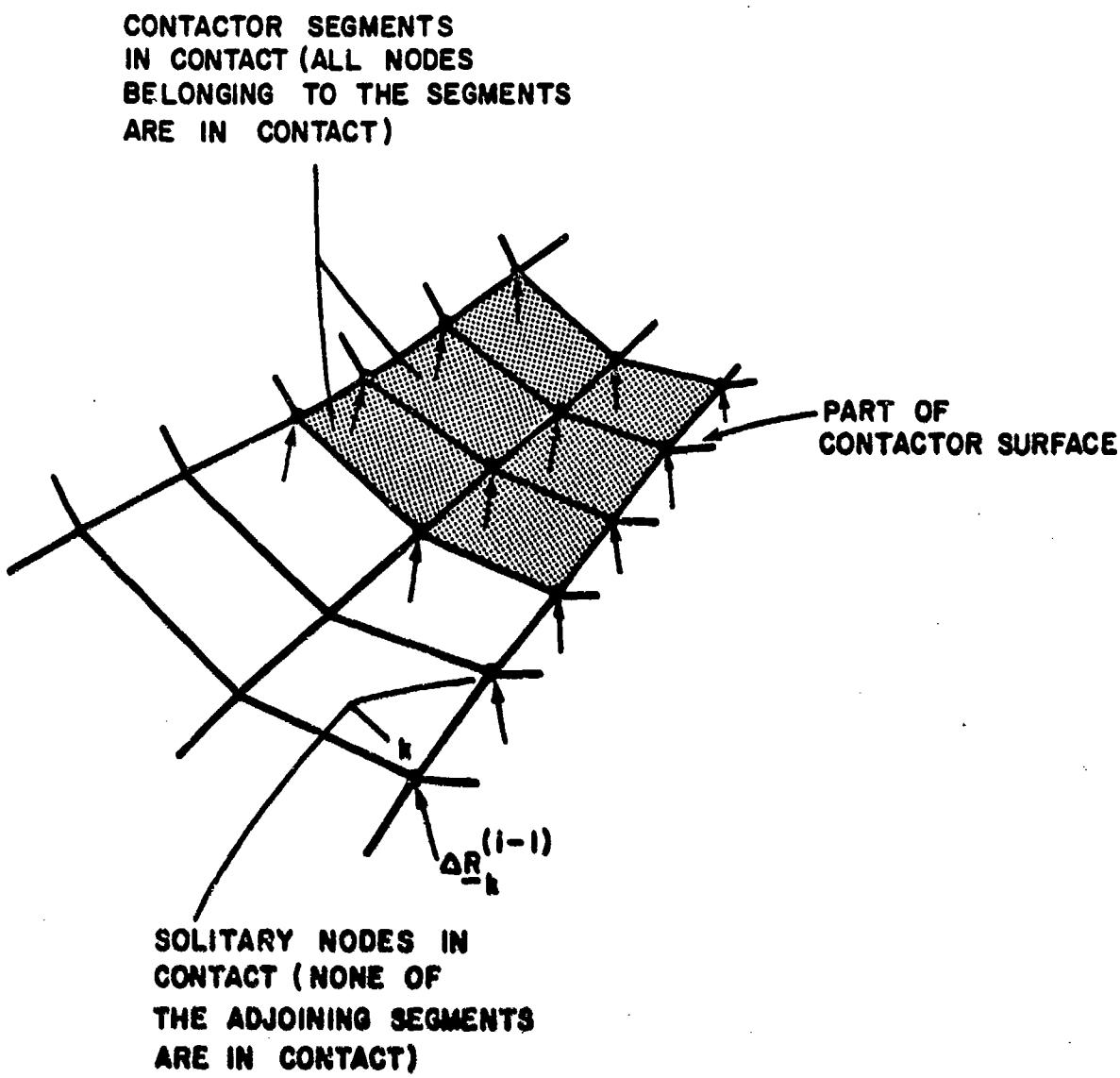

Figure 6 Contact region comprised of six contactor segments in contact and two solitary nodes in contact

For sliding contact

$$\underline{t+\Delta t}_{\underline{\lambda}_k}(i-1) = \underline{T}_n^k + \mu \frac{|\underline{T}_n^k|}{|\underline{T}_t^k|} \underline{T}_t^k \tag{52}$$

For sticking contact

$$\underline{t+\Delta t}_{\underline{\lambda}_k}(i-1) = \underline{\Delta R}_k(i-1). \tag{53}$$

2.6 Evaluation of the Conditions of Sticking, Sliding and Tension Release at the Contactor Nodes

Once the conditions of the contactor segments have been decided as discussed in Section 2.5.2, the algorithm determines the conditions of the contactor surface nodes as shown in Table 1.

For the solitary nodes in contact, the conditions at the nodes are given directly by the calculation of friction update.

A special case arises when a contactor node comes into contact with the target surface after iteration (i-1), while the node was not in contact after iteration (i-2). Its condition for iteration (i) is obtained as:

- sliding contact if the contact surfaces are frictionless
- sticking contact if the contact surfaces are frictional.

Using the conditions at the contactor nodes for iteration (i), the matrices $\underline{t+\Delta t}_{\underline{K}_\lambda}(i-1)$ and $\underline{t+\Delta t}_{\underline{\Delta}_c}(i-1)$ are evaluated (see Section 2.4). For iteration (i), the total number of contact equations is equal to the number of sliding contactor nodes plus three times the number of sticking contactor nodes.

III. SOLUTION METHOD FOR CONTACT-DYNAMICS

The solution of dynamic contact problems is obtained using the procedure discussed above for static analysis, but now including the effects of inertia and damping forces. Thus, the incremental equations of equilibrium for iteration (i) at time t+Δt are:

Table 1 STATE OF CONTACTOR NODE AS DECIDED BY STATES OF ADJOINING CONTACTOR SEGMENTS

STATE OF ADJOINING CONTACTOR SEGMENTS		STATE OF CONTACTOR NODE
One adjoining segment	Other adjoining segments	
Sticking	Sticking Sliding Tension release	Sticking
Sliding	Sliding Tension release	Sliding
Tension release	Tension release	Tension release

$$\begin{bmatrix} \underline{M} & \underline{0} \\ \underline{0} & \underline{0} \end{bmatrix} \begin{bmatrix} \Delta\ddot{\underline{U}}^{(i)} \\ \underline{0} \end{bmatrix} + \begin{bmatrix} \underline{C} & \underline{0} \\ \underline{0} & \underline{0} \end{bmatrix} \begin{bmatrix} \Delta\dot{\underline{U}}^{(i)} \\ \underline{0} \end{bmatrix} + \left[\begin{bmatrix} {}^{t+\Delta t}\underline{K}^{(i-1)} & \underline{0} \\ \underline{0} & \underline{0} \end{bmatrix} + \begin{bmatrix} \underline{0} & {}^{t+\Delta t}\underline{K}_{\lambda}{}^{(i-1)} \\ {}^{t+\Delta t}\underline{K}_{\lambda}{}^{(i-1)^T} & \underline{0} \end{bmatrix} \right] \begin{bmatrix} \Delta\underline{U}^{(i)} \\ \Delta\underline{\lambda}^{(i)} \end{bmatrix}$$

$$= \begin{bmatrix} {}^{t+\Delta t}\underline{R} \\ \underline{0} \end{bmatrix} - \begin{bmatrix} \underline{M} & \underline{0} \\ \underline{0} & \underline{0} \end{bmatrix} \begin{bmatrix} {}^{t+\Delta t}\ddot{\underline{U}}^{(i-1)} \\ \underline{0} \end{bmatrix} - \begin{bmatrix} \underline{C} & \underline{0} \\ \underline{0} & \underline{0} \end{bmatrix} \begin{bmatrix} {}^{t+\Delta t}\dot{\underline{U}}^{(i-1)} \\ \underline{0} \end{bmatrix} - \begin{bmatrix} {}^{t+\Delta t}\underline{F}^{(i-1)} \\ \underline{0} \end{bmatrix} + \begin{bmatrix} {}^{t+\Delta t}\underline{R}_{c}{}^{(i-1)} \\ {}^{t+\Delta t}\underline{\Delta}_{c}{}^{(i-1)} \end{bmatrix} \qquad (54)$$

where,

$\Delta\dot{\underline{U}}^{(i)}$ = Vector of incremental velocities in iteration (i)

$\Delta\ddot{\underline{U}}^{(i)}$ = Vector of incremental accelerations in iteration (i)

${}^{t+\Delta t}\dot{\underline{U}}^{(i-1)}$ = Vector of velocities after iteration (i-1)

${}^{t+\Delta t}\ddot{\underline{U}}^{(i-1)}$ = Vector of accelerations after iteration (i-1)

$\underline{M}$ = Mass matrix of the contactor and target bodies

$\underline{C}$ = Viscous damping matrix for the continua of the contactor and target bodies.

The evaluation of the contact matrices ${}^{t+\Delta t}\underline{K}_{\lambda}{}^{(i-1)}$ and ${}^{t+\Delta t}\underline{\Delta}_{c}{}^{(i-1)}$ is performed as in static analysis.

For the contactor surface nodes belonging to the region of contact, the contact forces after iteration (i) (prior to updating) are obtained as

$$\Delta\underline{R}^{(i-1)} = {}^{t+\Delta t}\underline{F}^{(i-1)} + \underline{M}\,{}^{t+\Delta t}\ddot{\underline{U}}^{(i-1)} + \underline{C}\,{}^{t+\Delta t}\dot{\underline{U}}^{(i-1)} - {}^{t+\Delta t}\underline{R}. \qquad (55)$$

This vector is used as described in Section 2.5 to evaluate the updated nodal point contact forces ${}^{t+\Delta t}\underline{R}_{c}{}^{(i-1)}$.

IV. ITERATION STRATEGY AND CONVERGENCE CRITERIA

For iteration (i) at time $t+\Delta t$, the sequence of calculations performed in the contact solution is as follows:

- Use the nodal forces $\Delta \underline{R}^{(i-1)}$ to recover segment tractions on the contactor surface. Update the segment tractions and the forces acting at the solitary nodes in contact to satisfy Coulomb's law of friction and calculate the updated contact surface forces ${}^{t+\Delta t}\underline{R}_c^{(i-1)}$ (see Section 2.5).

- Use the current geometry after iteration (i-1) to determine the target segment of contact for each contactor node belonging to the contact region. Also evaluate the material overlap and the area coordinates of the physical point of contact.

- Detect if any new contactor nodes have come into contact after iteration (i-1).

- Evaluate the states of the contactor nodes for iteration (i) (see Section 2.6).

- Evaluate the contact matrices ${}^{t+\Delta t}\underline{K}_\lambda^{(i-1)}$ and ${}^{t+\Delta t}\underline{\Delta}_c^{(i-1)}$ and assemble all matrices as given in Eq. (12). Then solve Eq. (12) to obtain the unknown quantities $\Delta \underline{U}^{(i)}$ and $\Delta \underline{\lambda}^{(i)}$.

  Note that the increments in contact forces, $\Delta \lambda^{(i)}$, obtained from the solution of Eq. (12) are not used subsequently in any calculation. The total contact forces (prior to updating) after each iteration are simply obtained as given by Eq. (23).

Convergence of solution is accepted after iteration (i) if the following criteria are simultaneously satisfied:

- Energy convergence criterion

$$\frac{\Delta \underline{U}^{(i)T}\left[{}^{t+\Delta t}\underline{R} - {}^{t+\Delta t}\underline{F}^{(i-1)} - \underline{M}\,{}^{t+\Delta t}\ddot{\underline{U}}^{(i-1)} - \underline{C}\,{}^{t+\Delta t}\dot{\underline{U}}^{(i-1)} + {}^{t+\Delta t}\underline{R}_c^{(i-1)}\right]}{\Delta \underline{U}^{(1)T}\left[{}^{t+\Delta t}\underline{R} - \underline{F} - \underline{M}\,{}^{t+\Delta t}\ddot{\underline{U}}^{(0)} - \underline{C}\,{}^{t+\Delta t}\dot{\underline{U}}^{(0)} + \underline{R}_c\right]} \leq \text{ETOL} \tag{56}$$

where ETOL is an energy convergence tolerance.

- Force convergence criterion

$$\frac{\left\| {}^{t+\Delta t}\underline{R} - {}^{t+\Delta t}\underline{F}^{(i-1)} - \underline{M}\,{}^{t+\Delta t}\underline{\ddot{U}}^{(i-1)} - \underline{C}\,{}^{t+\Delta t}\underline{\dot{U}}^{(i-1)} + {}^{t+\Delta t}\underline{R}_c^{(i-1)} \right\|_2}{RNORM} \leq RTOL \tag{57}$$

where RNORM is a reference force for convergence [7] and RTOL is a force convergence tolerance. In the evaluation of the Euclidean norm in Eq. (57), only the translational degrees of freedom are considered.

For the rotational degrees of freedom, a moment convergence criterion is specified in analogy to the force convergence criterion.

- Contact Force Convergence Criterion

$$\frac{\left\| \Delta\underline{R}^{(i-1)} - \Delta\underline{R}^{(i-2)} \right\|_2}{\left\| \Delta\underline{R}^{(i-1)} \right\|_2 + RCONSM} \leq RCTOL \tag{58}$$

where RCTOL is a contact force convergence tolerance and RCONSM is a small number. Note that RCONSM makes the denominator of Eq. (58) nonzero when $\left\| \Delta\underline{R}^{(i-1)} \right\|_2 = 0$ (i.e., no contact conditions exist during iteration (i-1)).

V. TIME INTEGRATION OF THE EQUILIBRIUIM EQUATIONS FOR DYNAMIC CONTACT

A valid dynamic contact solution must satisfy the following two criteria:

- The total energy of the system is conserved
- The impulse-momentum relationship is satisfied for each body.

Using the Newmark method of implicit time integration, the acceleration and velocity vectors after iteration (i-1) at time t+Δt are [3]

$$ {}^{t+\Delta t}\underline{\ddot{U}}^{(i-1)} = \frac{1}{\alpha(\Delta t)^2}\left({}^{t+\Delta t}\underline{U}^{(i-1)} - {}^{t}\underline{U}\right) - \frac{1}{\alpha\Delta t}\,{}^{t}\underline{\dot{U}} - \left(\frac{1}{2\alpha} - 1\right){}^{t}\underline{\ddot{U}} \qquad (59) $$

$$ {}^{t+\Delta t}\underline{\dot{U}}^{(i-1)} = {}^{t}\underline{\dot{U}} + \left[(1-\delta)\,{}^{t}\underline{\ddot{U}} + \delta\,{}^{t+\Delta t}\underline{\ddot{U}}^{(i-1)}\right]\Delta t \qquad (60) $$

where,

α, δ = Newmark parameters

${}^{t}\underline{U}, {}^{t}\underline{\dot{U}}, {}^{t}\underline{\ddot{U}}$ = displacement, velocity, and acceleration vectors at time t respectively

${}^{t+\Delta t}\underline{U}^{(i-1)}$ = displacement vector after iteration (i-1) at time t+Δt.

Also, the incremental acceleration and velocity vectors in iteration (i) are given by

$$ \Delta\underline{\ddot{U}}^{(i)} = \frac{1}{\alpha(\Delta t)^2}\,\Delta\underline{U}^{(i)} \qquad (61) $$

$$ \Delta\underline{\dot{U}}^{(i)} = \frac{\delta}{\alpha\Delta t}\,\Delta\underline{U}^{(i)}. \qquad (62) $$

Equations (59) to (62) are used in the incremental equations of equilibrium for dynamic contact (see Eq. (54)). Since the calculated response depends on the values of the Newmark parameters α and δ, the objective must be to choose optimum parameters for the solution.

In search for suitable α and δ parameters, the solutions to some simple numerical experiments of two unequal colliding point masses were considered.

The experiments were repeated for various combinations of impact velocities. The study showed that the criteria of energy and momentum balance are satisfied when $\alpha=\frac{1}{2}$ and $\delta=\frac{1}{2}$ are used. With other values of α and δ, the energy and momentum equations are not necessarily satisfied.

Another numerical experiment involves the longitudinal impact of two identical bars which are moving towards each other with a constant velocity (see Fig. 7a,b). The bar material is linear elastic and the contact surfaces are frictionless. For the solution obtained using $\alpha=\frac{1}{2}$ and $\delta=\frac{1}{2}$, the total energy of the bar (strain energy + kinetic energy) is conserved throughout the solution and the impulse-momentum relationship is satisfied. Good agreement is obtained between the numerical solution and the analytical solution [4] for the stress generated due to impact (see Fig. 7c).

In addition, the integration scheme with $\alpha=\frac{1}{2}$ and $\delta=\frac{1}{2}$ has the following desirable characteristics (considering linear analysis):

- The method is unconditionally stable since the condition $\alpha \geq \frac{1}{4}(\delta+\frac{1}{2})^2$ is satisfied.
- The scheme gives no amplitude decay, since $\delta = \frac{1}{2}$.
- The percentage period elongation is reasonably small.

VI. NUMERICAL SOLUTIONS

The algorithm presented in the previous sections was implemented in the computer program ADINA [7] and the results of some sample analyses are presented in this section. In these analyses, the primary objective was to study the performance of the algorithm under various conditions of contact.

6.1 Analysis of Axisymmetric Hertz Contact Problems

A sphere of radius R=5 is considered to come into contact with a flat rigid surface (see Fig. 8). The analysis is performed for the following two conditions:

- Static analysis of contact when the sphere is subjected to an externally applied total force $P=-523\underline{k}$ (see Fig. 8a)

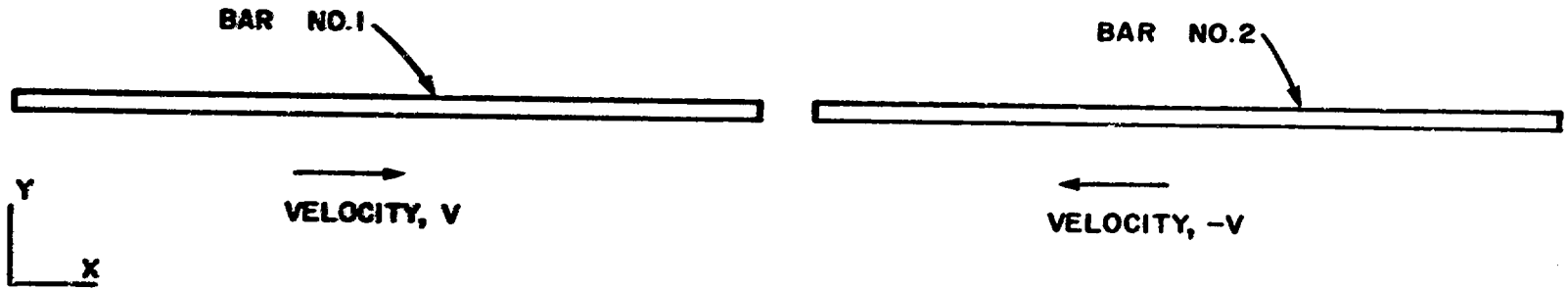

BARS 1 AND 2 ARE IDENTICAL

$E = 1000.0$ $\rho = 0.001$

AREA = 1.0 LENGTH = 100

VELOCITY, $V = 1.0\,\underline{i}$

a) Problem considered

Figure 7 Analysis of longitudinal impact of identical bars

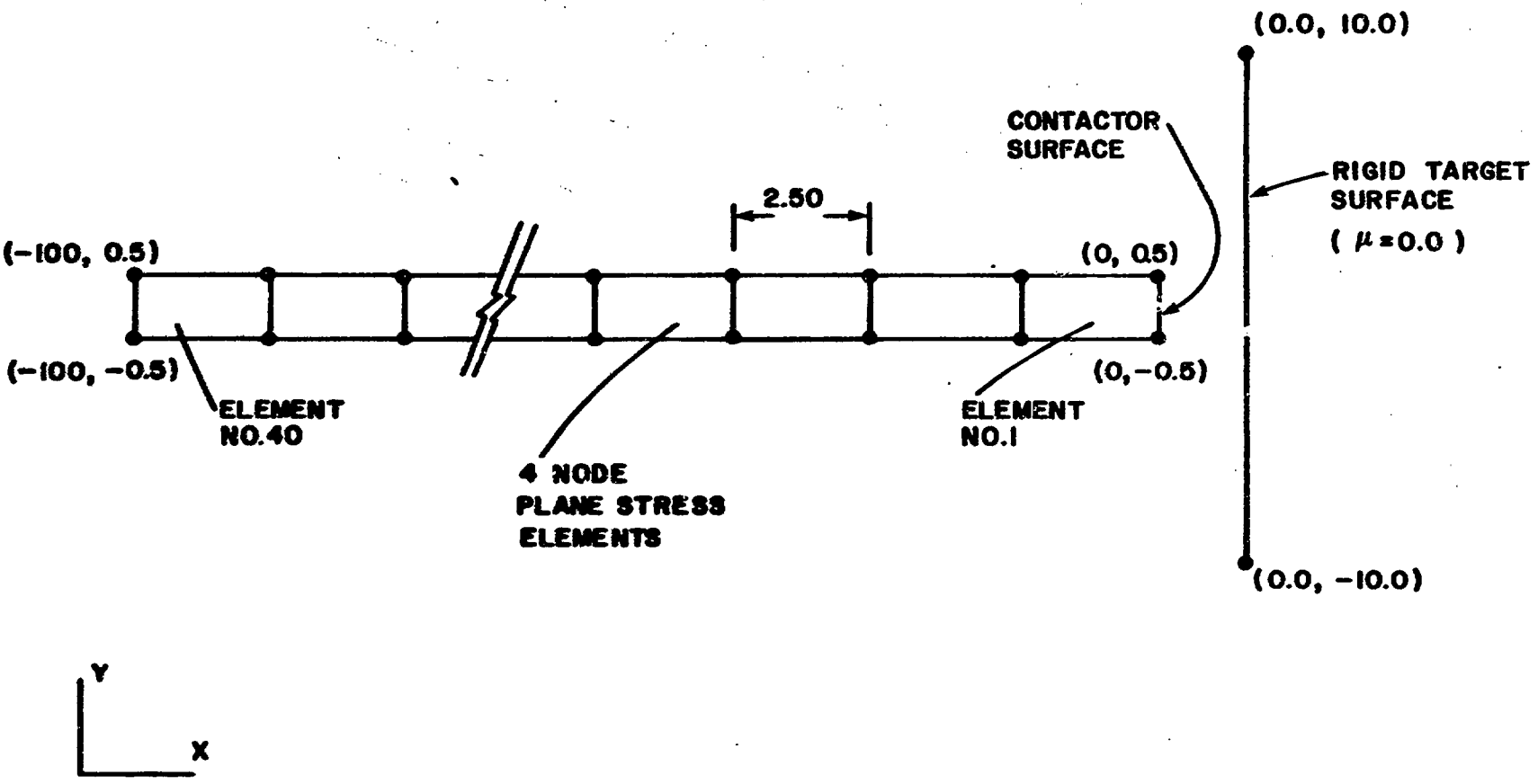

b) Finite element model

Figure 7 Continued

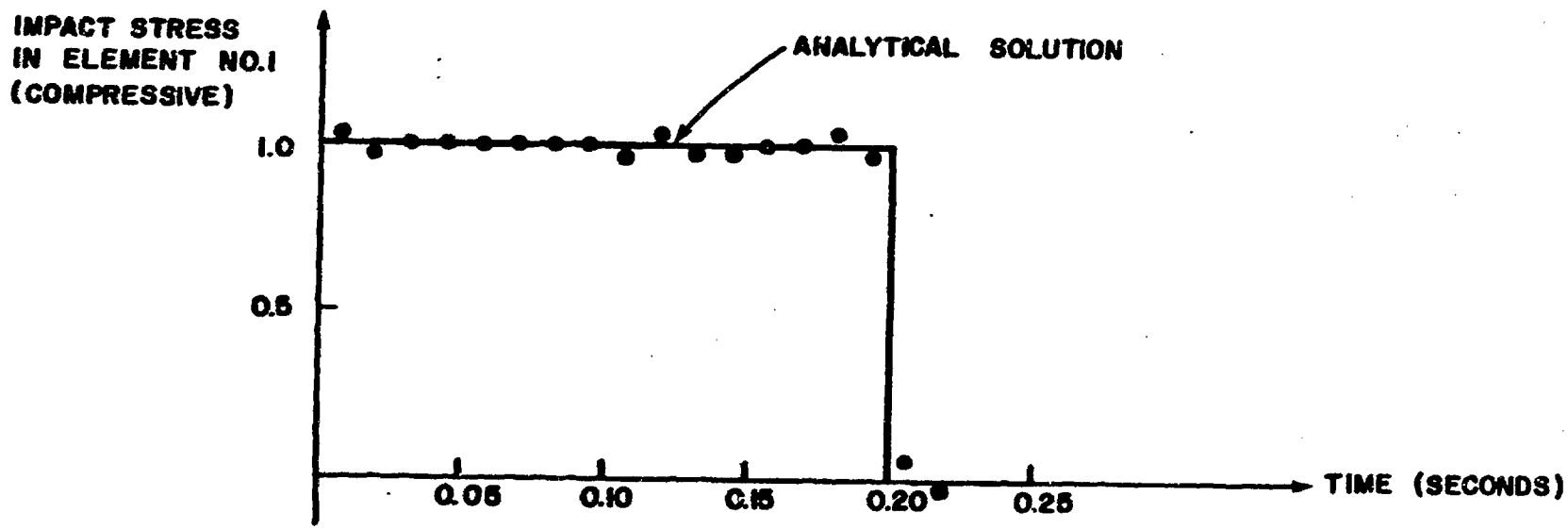

c) Impact stress in element number 1. Each solution point is the average element stress over a time interval 0.0125 seconds. The time step used is $\Delta t=0.00025$ seconds.

Figure 7 *Continued*

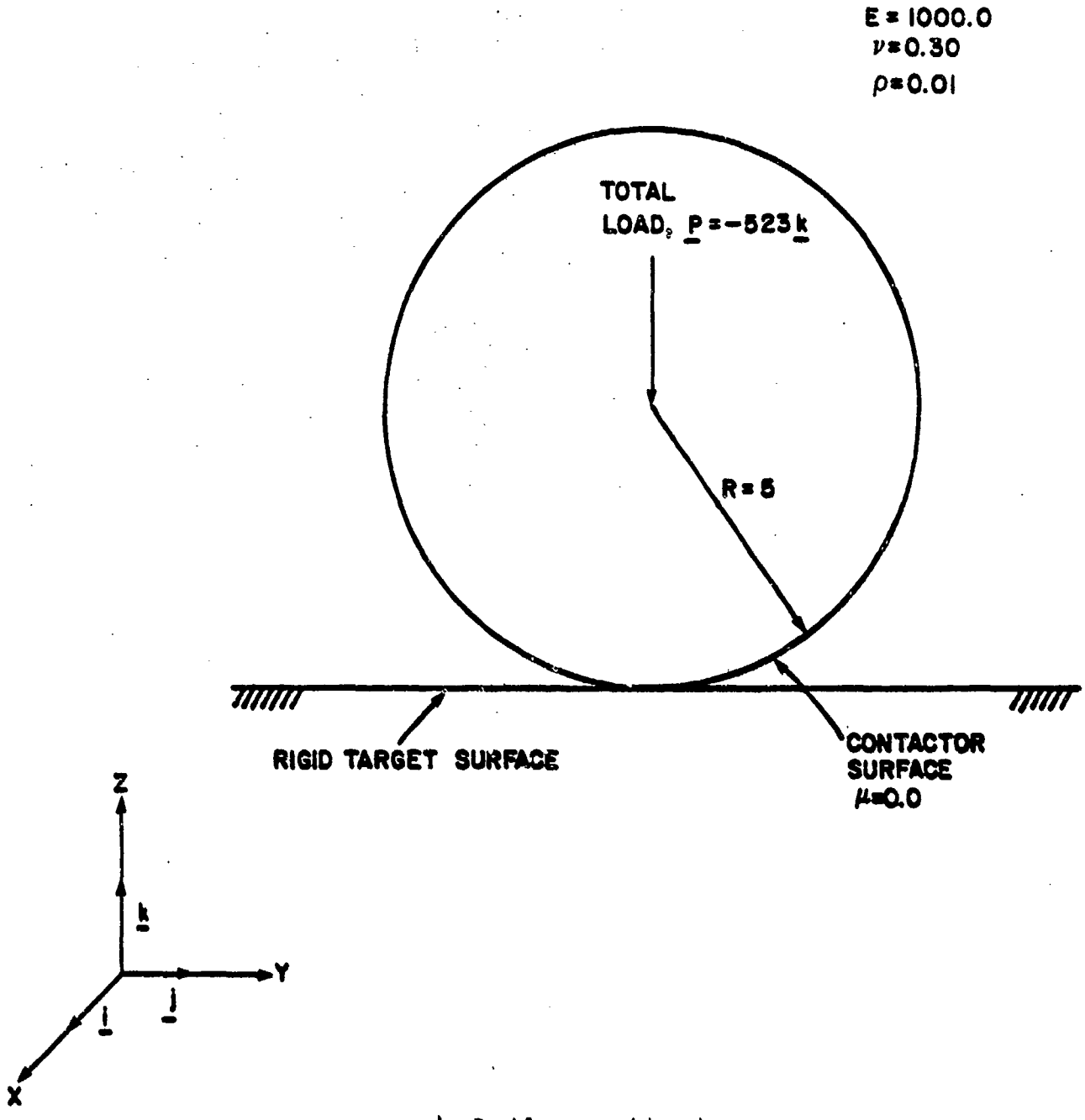

a) Problem considered

Figure 8 Analysis of Hertz axisymmetric contact problem
(M.N.O. formulation denotes materially-nonlinear-only formulation [3])

- Dynamic analysis of contact when the sphere impacts the rigid surface. Prior to impact, the sphere has an initial velocity V=-3$\underline{k}$.

6.1.1 Finite Element Discretization

Due to symmetry of the sphere geometry and the applied loading, only a thin wedge from the sphere continuum is discretized (see Fig. 8b,c). The wedge is bounded by its two semicircular sides and the enclosed wedge angle is 1 degree. The wedge is discretized using eight node 3-D solid elements. For each node on Face 1 of the wedge, the degree-of-freedom normal to Face 1 (i.e., along the skew coordinate direction y_1) is deleted. Similarly, for each node on Face 2 of the wedge, the degree-of-freedom normal to Face 2 (i.e., along the skew coordinate direction y_2) is deleted.

The contactor surface is defined over the wedge boundary (see Fig. 8b). The target surface is defined to be the flat rigid surface, which is modeled by specifying target nodes with no degrees of freedom. In an X—Y plane view, the target surface is triangular in shape.

6.1.2 Static Analysis

The wedge is subjected to a uniformly distributed body force along the negative z direction such that the resultant of the body force corresponds to P=-523$\underline{k}$ acting at the center of the sphere (i.e., the total force applied onto the wedge equals -(523/360)$\underline{k}$).

Figure 9 shows the calculated contact tractions and a comparison with the Hertz analytical solution [5].

6.1.3 Dynamic Analysis

For all nodes belonging to the wedge, an initial velocity V=-3$\underline{k}$ was assigned. The time integration of the dynamic response was performed using the Newmark parameters $\alpha=\frac{1}{4}$ and $\delta=\frac{1}{2}$ (see Section 5). The time step was equal to $\Delta t=0.01$ sec.

Figure 10 shows the calculated contact tractions and a comparison with the Hertz analytical solution [5].

6.2 Analysis of Compressed Spheres Subjected to a Torsional Moment

Figure 11 shows two identical spheres which are first compressed onto each other (P=-222k) and then subjected to a twisting moment(M=52$\underline{k}$). The coefficient of friction is very large (infinite).

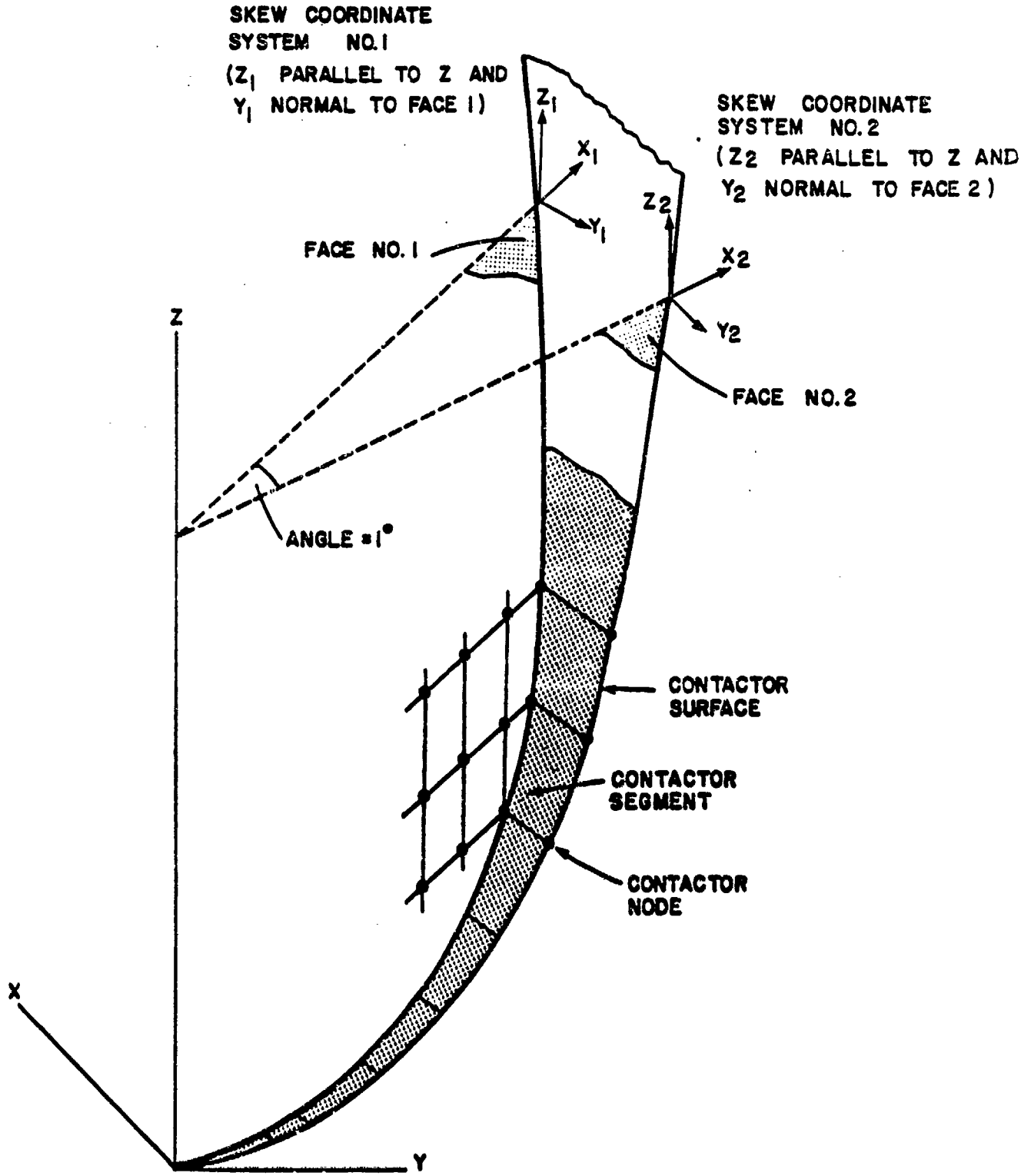

b) A wedge from the sphere continuum considered in the analysis

Figure 8 Continued

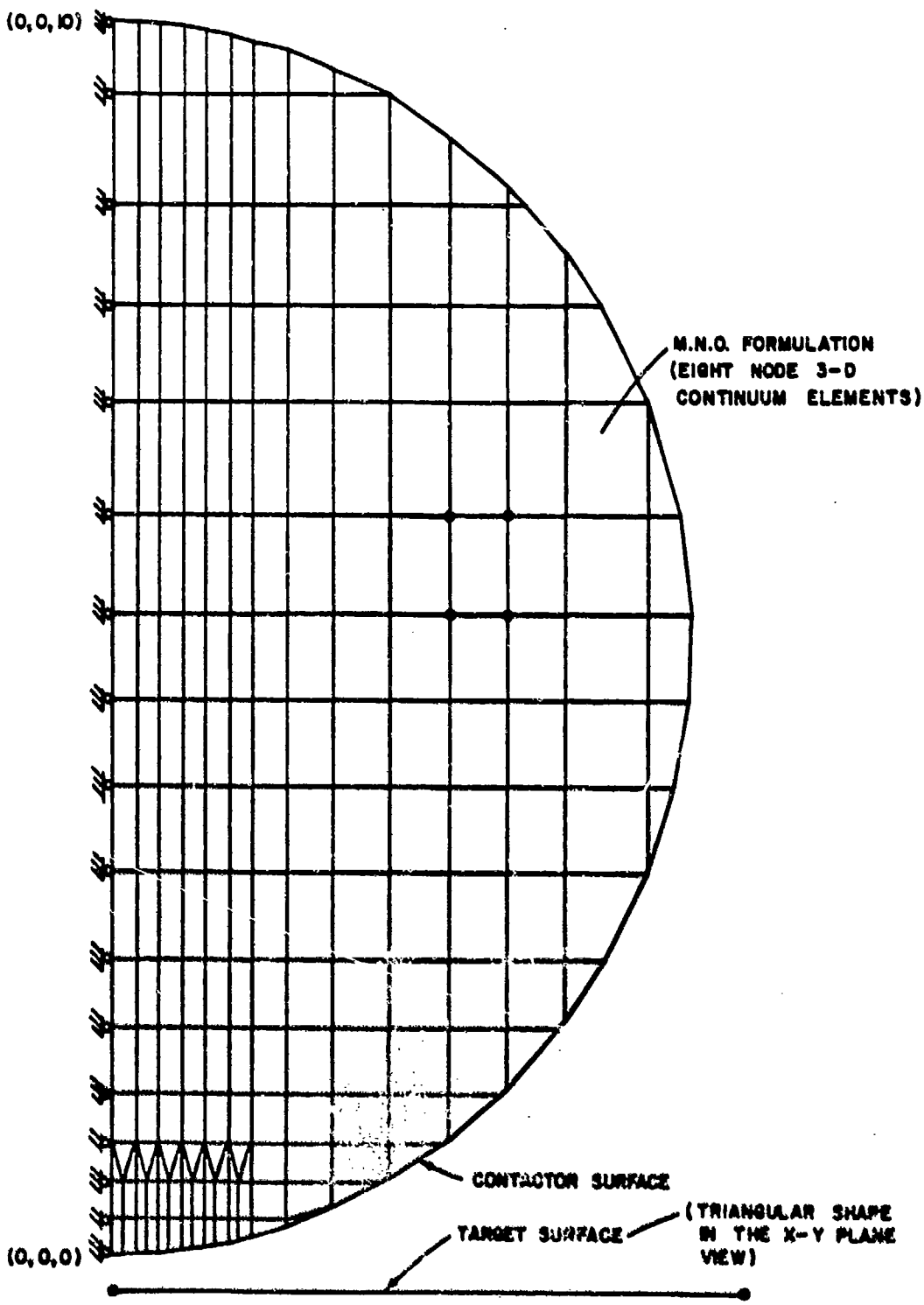

c) Finite element discretization of the wedge (x_1—z_1 plane view). One 3-D element is used across the wedge thickness (see Fig. 8b).

Figure 8 Continued

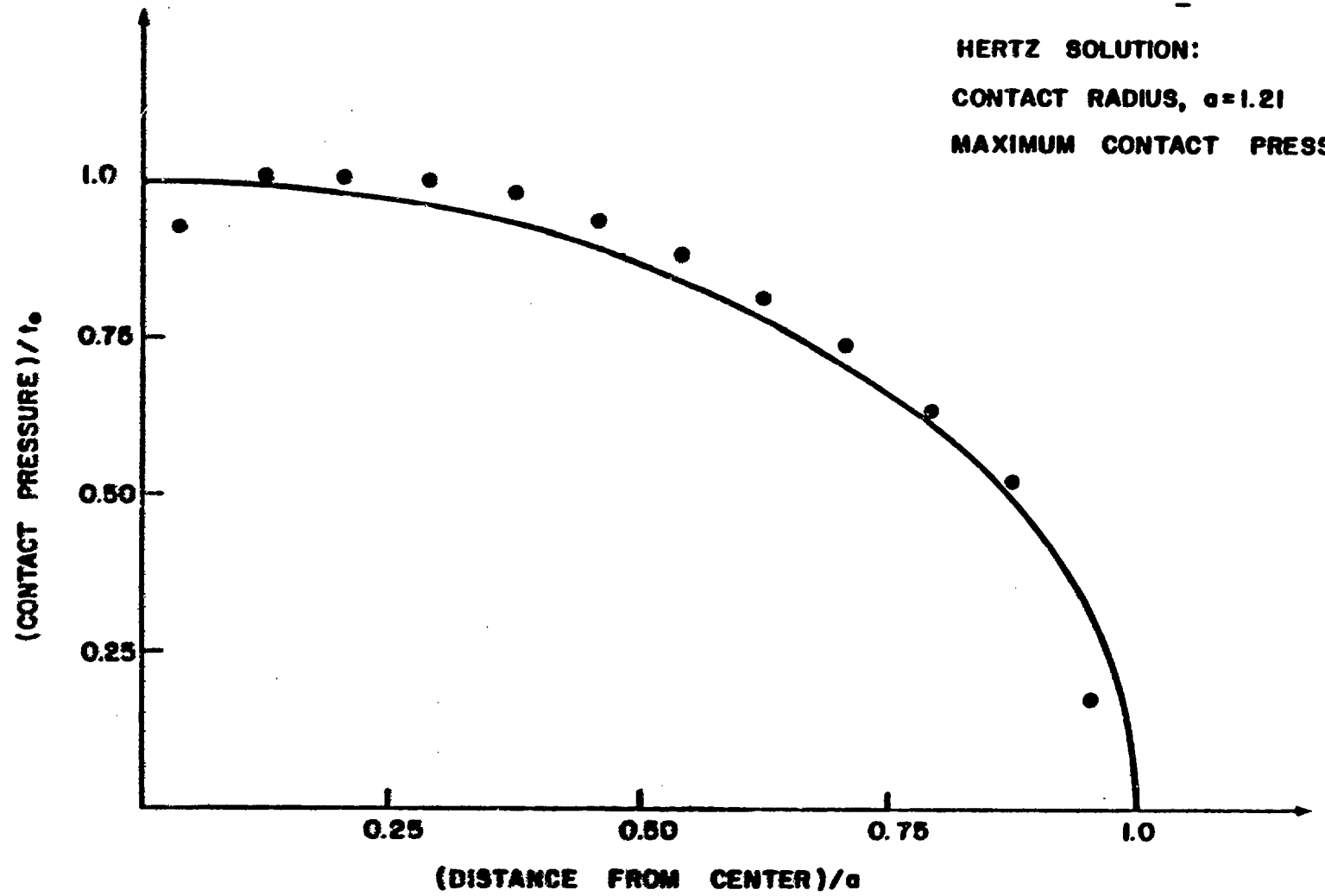

Figure 9 Solution to the Hertz axisymmetric contact problem (statics)

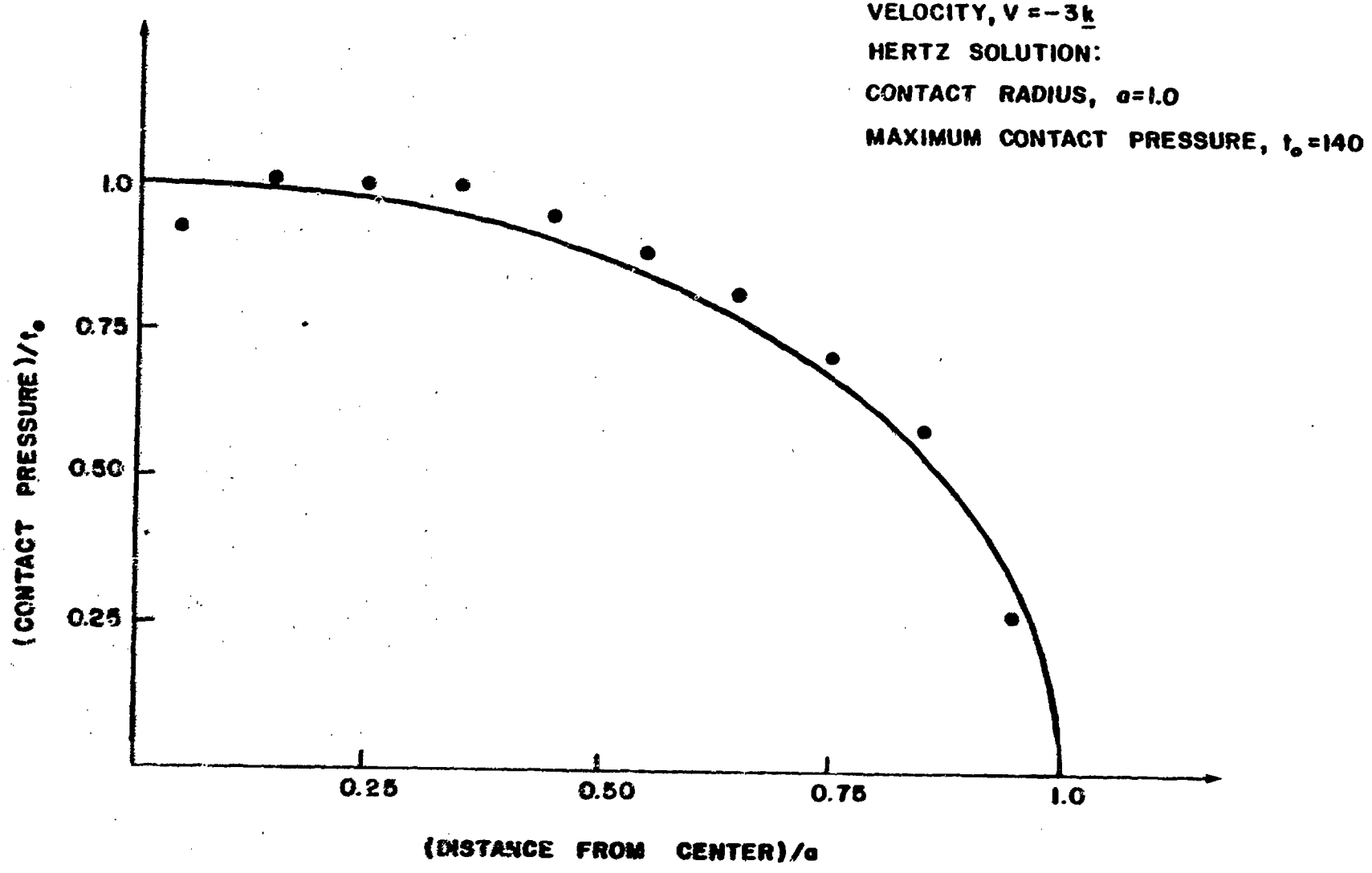

Figure 10 Solution to the Hertz axisymmetric contact problem (dynamics)

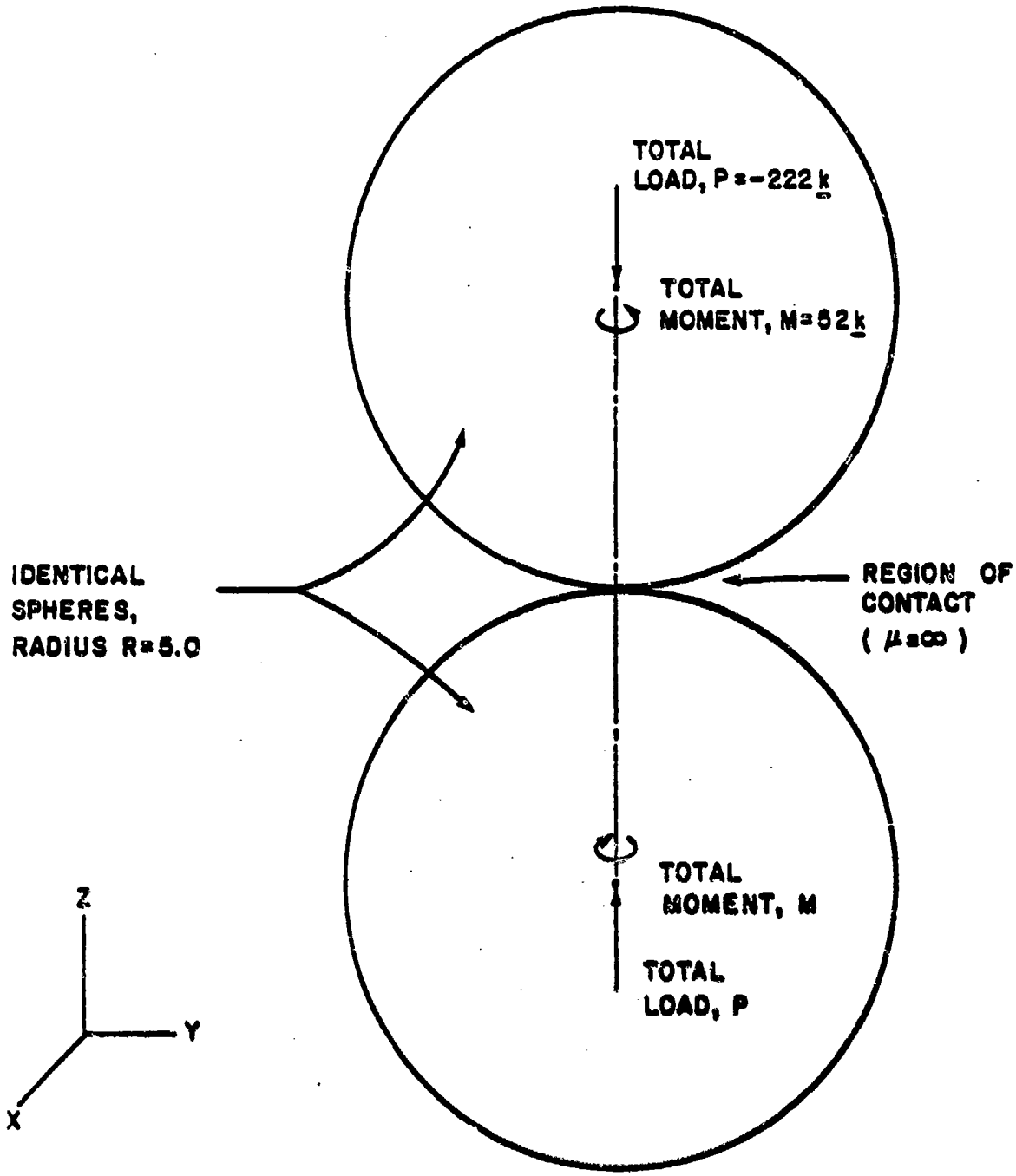

Figure 11 Analysis of compressed spheres subjected to a torsional moment

Due to the symmetry in geometry and the skew symmetry of the applied loading, we can model the problem by considering a single sphere first compressed onto a flat rigid surface and then subjected to a twisting moment. This sphere is modeled as a thin wedge, as in the solutions of Section 6.1.

The finite element model of the wedge is as shown in Figs. 8b,c. To enforce the condition of skew-symmetry, the x_1,y_1, and z_1 displacements of the nodes on Face 1 are constrained to be respectively equal to the x_2,y_2, and z_2 displacements of the corresponding nodes on Face 2.

The wedge is first subjected to a uniformly distributed body force along the negative z direction such that the resultant of the body force corresponds to $P=-222\underline{k}$ acting at the center of the sphere. As a result, a region of contact between the sphere and the rigid surface is established (radius of contact=0.9).

To apply the twisting moment, the wedge is subjected to a distributed lateral body force such that at any point (x,y,z) within the wedge, the body force per unit volume, $\underline{b}$, is

$$\underline{b} = C\, r\, \underline{i}_\theta \tag{63}$$

where,

$$C = \text{constant}$$

$$r = \sqrt{x^2 + y^2} \tag{64}$$

$$= \text{distance of point } (x,y,z) \text{ from the Z axis}$$

$$\underline{i}_\theta = -\frac{y}{r}\,\underline{i} + \frac{x}{r}\,\underline{j} \tag{65}$$

$$= \text{unit vector orthogonal to } x\underline{i} + y\underline{j}$$

For C=0.01, the applied lateral body force corresponds to a total twisting moment $M=52\underline{k}$ applied to the sphere.

Figure 12 shows the calculated shearing traction in the contact region and a comparison with the analytical solution [6].

6.3 Dynamic Analysis of Frictional Sliding of a Point Mass

Figure 13 shows a mass, m=0.2, attached to two identical springs which are anchored to a flat rigid surface. The rigid surface lies in the X—Y plane and the mass rests on the surface. The coefficient of friction between the mass and the surface is 0.15. Both springs have the same linear force-deflection relationship and geometric nonlinearities are included in the analysis.

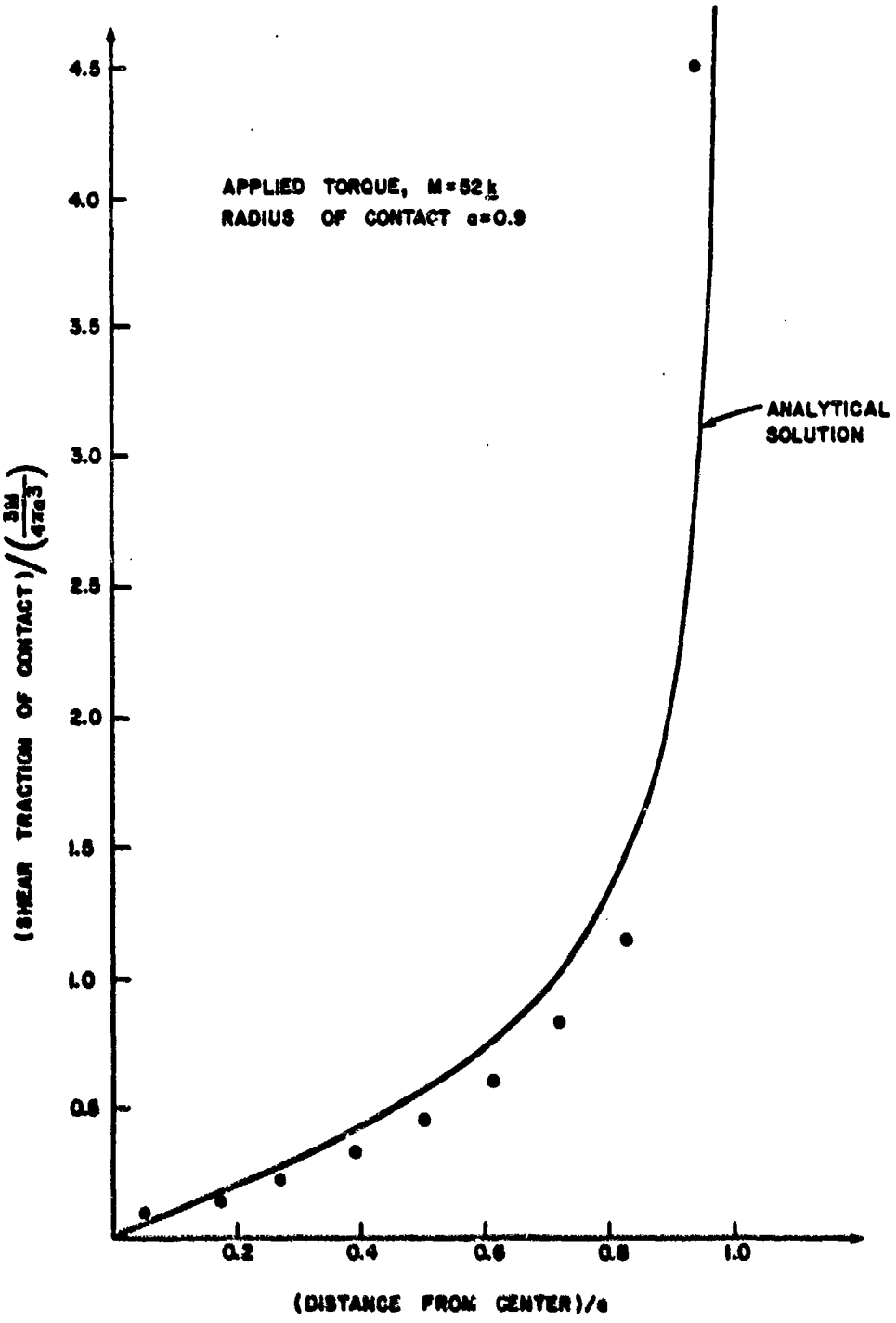

Figure 12 Solution to the problem of compressed spheres subjected to a twisting moment

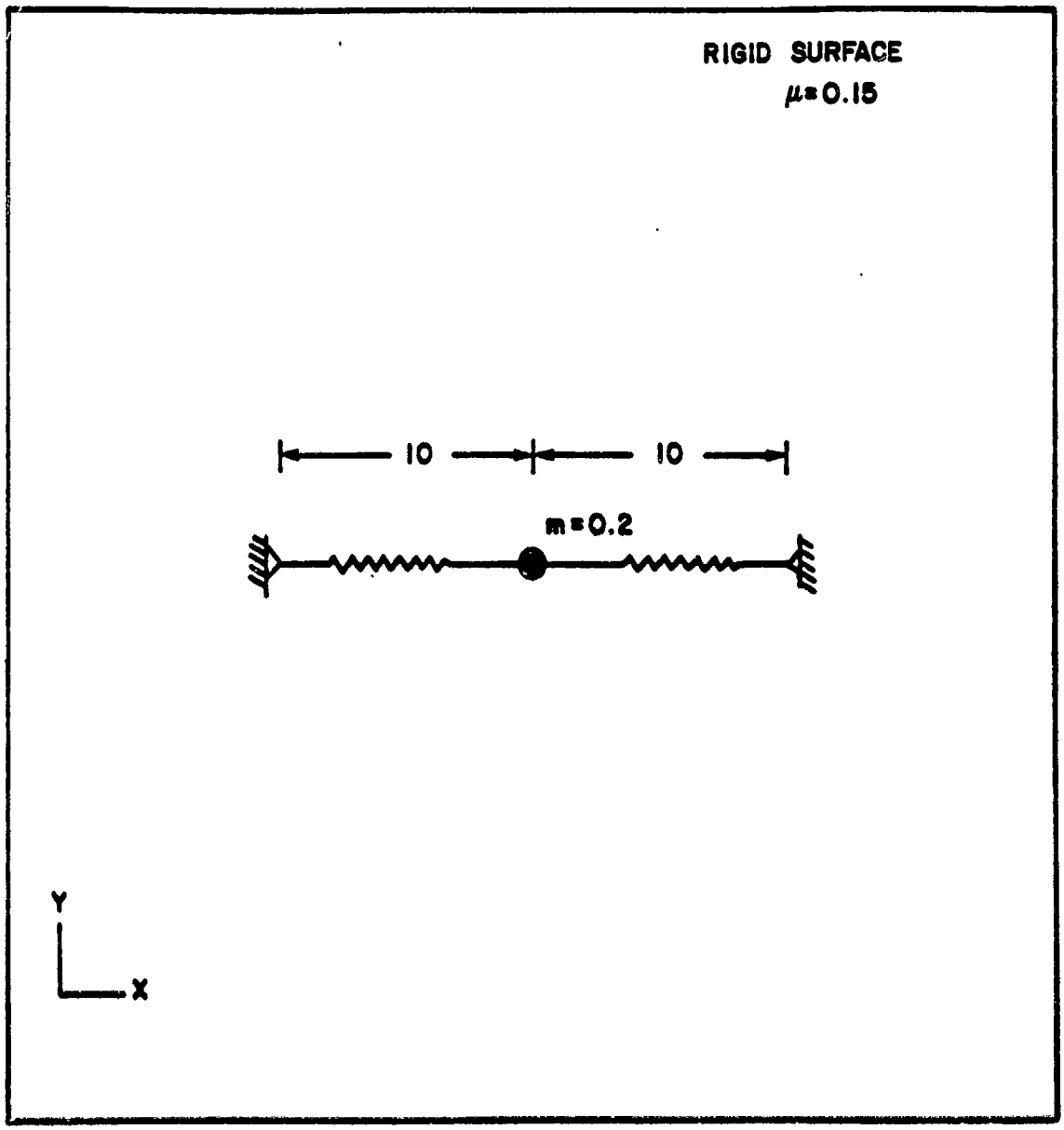

SPRINGS
E=1000.0
A=1.0

ACCELERATION
DUE TO GRAVITY=-10k

a) Problem considered

Figure 13 Dynamic analysis of frictional sliding of a point mass

The following two cases are considered to study effects of friction on the vibrations of the mass-spring system:

- The point mass is given an initial velocity of -1.0$\underline{i}$ and is then released. The movement of the mass takes place along the x-direction and the motion is resisted by the developed frictional force (when the mass is moving along the positive x direction, the frictional force acting on the mass equals -0.30$\underline{i}$).

- The point mass is given an initial displacement of -2.0$\underline{j}$ and is then released. The movement of the mass takes place along the y direction and the motion is resisted by the developed frictional force (when the mass is moving along the positive y direction, the frictional force acting on the mass equals -0.30$\underline{j}$).

Target Surface The flat rigid surface is chosen to be the target surface and is modeled using four nodes each with no degrees of freedom.

Contactor Surface The mass-spring system is chosen to be the contactor body. An auxiliary node (fixed in space) is used to define the contactor surface consisting of two contactor segments (see Figure 13b). The auxiliary node lies outside the region of the rigid target surface and thus is not in contact throughout the analysis. As a result, nodes 1,2, and 3 are treated as solitary nodes in contact. The direction of the normal vector at the solitary nodes is obtained from the geometry of the contactor segments.

Figure 14 shows the numerical results for the two cases considered. The obtained solutions satisfy the criteria of energy and momentum balance and, for each case, the work done by the frictional force equals the difference between the initial energy and the final energy of the system.

VII. CONCLUDING REMARKS

An algorithm for the solution of static and dynamic three-dimensional contact problems has been presented. The solution procedure uses a Lagrange multiplier technique to incrementally impose the constraints of compatible surface displacements due to contact. The contact forces are evaluated from distributed tractions that act on the contacting surfaces. These tractions are evaluated from the nodal point forces, which correspond to the internal element stresses and the externally applied loading, and the frictional conditions based on Coulomb's law. Some solution results obtained using the algorithm have been presented to demonstrate the applicability and performance of the solution procedure.

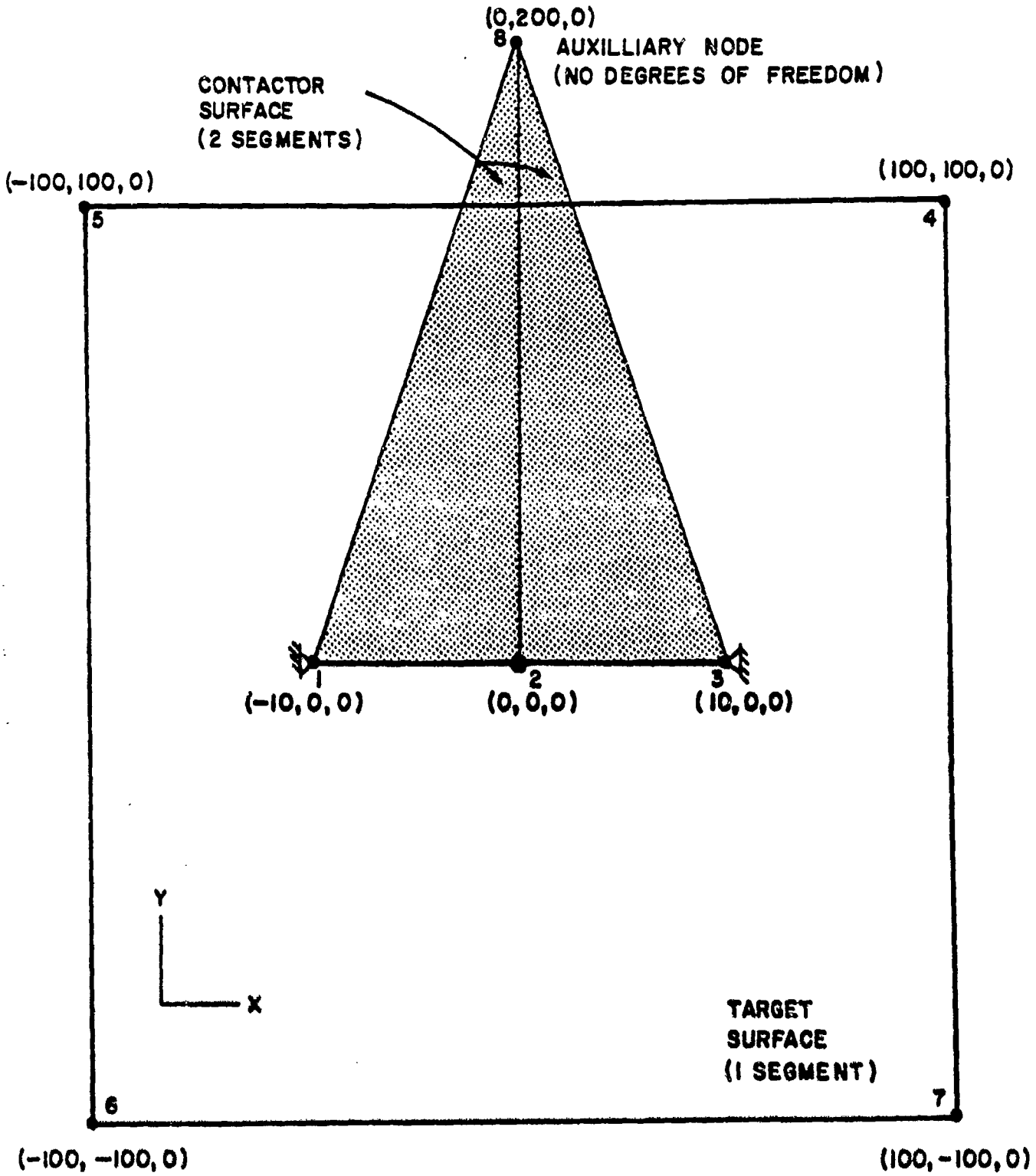

b) Finite element model used. All nodes except node 2 have all degrees of freedom deleted.

Figure 13 Continued

a) Case 1 (time step $\Delta t=0.001$ seconds)

Figure 14 Displacement time history of the sliding mass

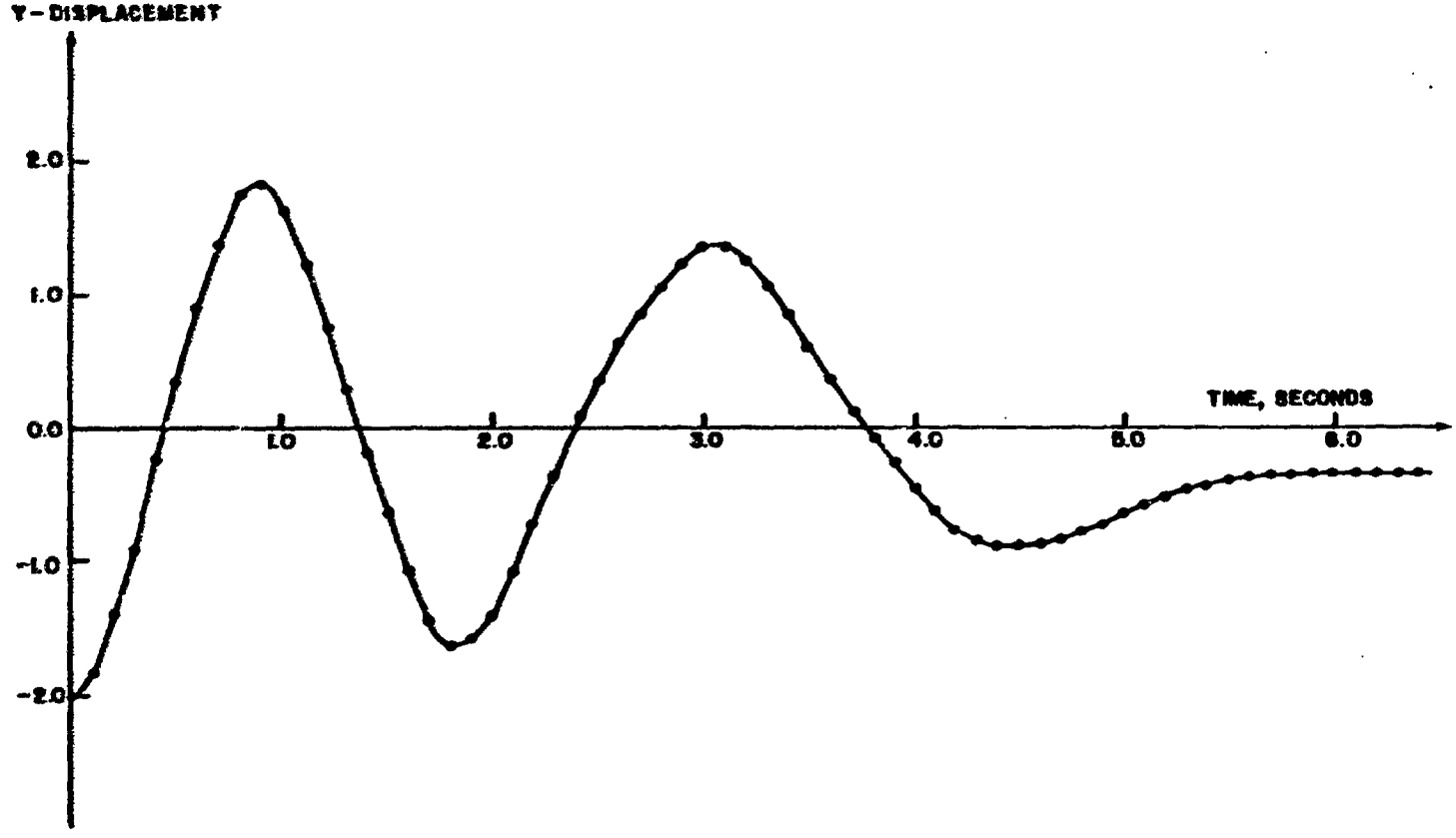

b) Case 2 (time step Δt=0.0025 seconds)

Figure 14 Continued

Using the algorithm already a wide variety of contact problems can be analyzed. However, there is an ever increasing need to solve more complex contact problems and additional research should be performed to broaden the applicability and effectiveness of the algorithm. This research should focus, for example, on the following items:

- Line searching in equilibrium iterations in the presence of contact.
- Development of the algorithm for explicit time integration.
- Improvement and evaluation of accuracy and effectiveness of implicit and explicit time integration schemes for dynamic contact.
- Modeling of contact surfaces using higher order surface segments.
- Evaluation of various friction laws and corresponding implementation for improved modeling of interface conditions and solution effectiveness.

These studies would be very useful to gain a deeper understanding of contact phenomena.

REFERENCES

1. K. J. Bathe and A. B. Chaudhary, "A Solution Method for Planar and Axisymmetric Contact Problems," Int. J. Numer. Methods Eng. (in press).

2. K. J. Bathe and A. B. Chaudhary, "On the Finite Element Analysis of Large Deformation Frictional Contact Problems," 7th Invitational Symposium on the Unification of Finite Elements, Finite Differences and Calculus of Variations, University of Connecticut, Storrs, 1984.

3. K. J. Bathe, "Finite Element Procedures in Engineering Analysis," Prentice Hall, 1982.

4. W. Johnson, "Impact Strength of Materials," Edward Arnold Publishers, 1972.

5. S. P. Timoshenko and J. N. Goodier, "Theory of Elasticity," McGraw-Hill, 1970.

6. J. J. O'Connor, "Compliance Under a Small Torsional Couple of an Elastic Plate Pressed Between Two Identical Elastic Spheres," J. of App. Mech., Vol. 33 , 1966.

7. "ADINA - A Finite Element Program for Automatic Dynamic Incremental Nonlinear Analysis," Report 81-1, ADINA Engineering, Watertown, MA 02172, and Vasteras, Sweden.

LIST OF SYMBOLS

$\underline{I}$	Identity matrix.
A_j	Area of segment j.
$\underline{C}$	Viscous damping matrix for the continua of the contactor and target bodies.
ETOL	Energy convergence tolerance.
$^{t+\Delta t\ (i-1)}\underline{F}_k$	Elements of vector of nodal point forces equivalent to element stresses after iteration (i-1) corresponding to degrees of freedom of node k.
$\underline{G}$	Coefficient matrix relating nodal values of segment tractions to the corresponding consistent nodal loads. $= \underline{H}^T \underline{J} \underline{H}$
$\underline{H}$	Matrix of values of the bilinear interpolation function at the Gaussian integration points.
$\underline{J}$	Diagonal matrix of values of the Jacobian determinant at The Gaussian integration points.
$^{t+\Delta t\ (i-1)}\underline{K}$	Tangent stiffness matrix including material and geometric nonlinearities after iteration (i-1).
$^{t+\Delta t\ (i-1)}\underline{K}_C$	Tangent stiffness matrix for the contactor body after iteration (i-1).
$^{t+\Delta t\ (i-1)}\underline{K}_T$	Tangent stiffness matrix for the target body after iteration (i-1).
$^{t+\Delta t\ (i-1)}\underline{K}_\lambda$	Contact matrix to include the constraints of compatible surface displacements after iteration (i-1).
$\underline{M}$	Mass matrix of the contactor and target bodies.
RTOL	Force convergence tolerance.
$^{t+\Delta t}\underline{R}_k$	Elements of vector of total applied external forces at time $t+\Delta t$ corresponding to the degrees of freedom of node k.
RCTOL	Contact force convergence tolerance.
ΔR_x^k	x-component of the consistent nodal load at node k due to the distributed segment tractions over segment j.
$\Delta \underline{R}_j$	Consistent nodal point force vectors corresponding to the segment tractions.
ΔR_x^k	x-component of the consistent nodal load at node k due to the distributed segment tractions over segment j only.

$\underline{\Delta R}_k^{(i-1)}$	Out-of-balance force vector at iteration (i-1).
$\underline{T}_n^j$	Total normal segment contact force.
$\underline{T}_t^j$	Total tangential segment contact force.
T_f^j	Total segment frictional capacity.
$\underline{T}^j$	Total segment contact force.
$\Delta \dot{U}^{(i)}$	Vector of incremental velocities in iteration (i).
$\Delta \ddot{U}^{(i)}$	Vector of incremental accelerations in iteration (i).
$t+\Delta t\dot{U}^{(i-1)}$	Vector of velocities after iteration (i-1).
$t+\Delta t\ddot{U}^{(i-1)}$	Vector of accelerations after iteration (i-1).
$\underline{b}$	Body force per unit volume.
i,j,k	Unit vectors along coordinate axes.
$\underline{t}_n^j$	Nodal point values of the normal component of the recovered segment tractions.
$\hat{\underline{t}}_t^j$	Nodal point values of the updated tangential segment traction.
$\hat{\underline{t}}_j$	Matrix of updated nodal point values of segment tractions.
$t_U, \dot{t}_U, \ddot{t}_U$	Displacement, velocity, and acceleration vectors at time t respectively.
$\underline{n}_j^C$	Normal vector to the contactor segment j.
$\underline{n}_j^T$	Normal vector to the target segment j.
t_x^k	X-component of the segment traction at node k.
$\underline{t}_j$	Nodal point values of the segment tractions.

$\underline{x}_k^{t+\Delta t\,(i)}$	Current global coordinates of a point or a node k at time $t+\Delta t$ at iteration (i).
$\Delta\underline{u}_k^{(i)}$	Vector of incremental displacement of node k in iteration (i).
α, δ	Newmark parameters.
$\alpha^i\ \beta^i\ \gamma^i$	Triangular area coordinates of point at iteration i.
$\underline{A}_j$	Matrix of consistent segment nodal point forces corresponding to the updated tractions over segment j.
μ	Coefficient of friction.
$\Delta\underline{\lambda}_k^{(i)}$	Vector of increments in contact forces at contactor node k in iteration (i).
$\underline{\lambda}_k^{t+\Delta t\,(i-1)}$	Contact force at contactor node k after iteration (i-1) corresponding to the x,y and z coordinate axes.
$\underline{\Delta}_k^{t+\Delta t\,(i)}$	Vector of material overlaps at contactor node k at iteration (i).

DISTRIBUTION LIST

No. of Copies	Organization
12	Administrator Defense Technical Info Center ATTN: DTIC-DDA Cameron Station Alexandria, VA 22314
1	Director of Defense Research & Engineering ATTN: DD/TWP Washington, DC 20301
1	Asst. to the Secretary of Defense (Atomic Energy) ATTN: Document Control Washington, DC 20301
1	Director Defense Advanced Research Projects Agency ATTN: Tech Lib 1400 Wilson Boulevard Arlington, VA 22209
2	Director Federal Emergency Management Agency ATTN: Mr. George Sisson/RF-SR Technical Library Washington, DC 20301
1	Director Defense Intelligence Agency ATTN: DT-2/Wpns & Sys Div Washington, DC 20301
1	Director National Security Agency ATTN: F. F. Butala, R15 Ft. George G. Meade, MD 20755
1	Director Joint Strategic Target Planning Staff JCS Offut AFB Omaha, NB 68113
1	HQDA ATTN: DAMA-ART-M Washington, DC 20310
1	Director Defense Communications Agency ATTN: 930 Washington, DC 20305
11	Director Defense Nuclear Agency ATTN: DDST/Dr. Conrad SPAS/P. R. Rohr SPSS/K. Goering G. Ullrich SPTD/T. Kennedy SSTL/Tech Lib (2 cys) STSI/Archives STSP/COL Kovel NATD NATA Washington, DC 20305
2	Commander Field Command, DNA ATTN: FCPR FCTMOF Kirtland AFB, NM 87115
1	Commander Field Command, DNA Livermore Branch ATTN: FCPRL P.O. Box 808 Livermore, CA 94550
1	Director Inst for Defense Analyses ATTN: IDA Librarian, 1801 Beauregard Street Alexandria, VA 22311
1	Commander US Army Materiel Command ATTN: AMCDRA-ST 5001 Eisenhower Avenue Alexandria, VA 22333

DISTRIBUTION LIST

No. of Copies	Organization
1	Commander US Army Development and Employment Agency ATTN: MODE-TED-SAB Fort Lewis, WA 98433
2	Director US Army BMD Advanced Technology Center P.O. Box 1500 ATTN: CDRABH-X CRDABH-S Huntsville, AL 35807
1	Program Manager US Army BMD Program Office ATTN: John Shea 5001 Eisenhower Avenue Alexandria, VA 22333
1	Commander US Army BMD Command ATTN: BDSMC-TFN/N.J. Hurst P.O. Box 1500 Huntsville, AL 35807
1	Commander US Army Engineer Division ATTN: HNDED-FD P.O. Box 1600 Huntsville, AL 35807
2	Deputy Chief of Staff for Operations and Plans ATTN: Technical Library Director of Chemical & Nuc Operations Department of the Army Washington, DC 20310
2	Office, Chief of Engineers Department of the Army ATTN: DAEN-MCE-D DAEN-RDM 890 South Pickett Street Alexandria, VA 22304
3	Commander US Army Engineer Waterways Experiment Station ATTN: Technical Library William Flathau Leo Ingram P.O. Box 631 Vicksburg, MS 39180
1	Commander US Army Engineering Center ATTN: ATSEN-SY-L Fort Belvoir, VA 22060
2	US Army Belvoir R&D Center ATTN: AMDME-EM, D. Frink, W. Comayne Fort Belvoir, VA 22060
1	Commander Armament R&D Center US Army AMCCOM ATTN: SMCAR-TDC Dover, NJ 07801
1	Commander Armament R&D Center US Army AMCCOM ATTN: SMCAR-TSS Dover, NJ 07801
1	Commander US Army Armament Munitions and Chemical Command ATTN: SMCAR-ESP-L Rock Island, IL 61299
1	Director Benet Weapons Laboratory Armament R&D Center US Army AMCCOM ATTN: SMCAR-LCB-TL Watervliet, NY 12189
10	CIA/ Office of Central Reference Dissemination Branch Room GE-47 HQS Washington, D.C. 20502

DISTRIBUTION LIST

No. of Copies	Organization
1	Commander US Army Aviation Research and Development Command ATTN: AMSAV-E 4300 Goodfellow Boulevard St. Louis, MO 63120
1	Director US Army Air Mobility Research and Development Laboratory Ames Research Center Moffett Field, CA 94035
1	Commander US Army Communications-Electronics Command ATTN: AMSEL-ED Fort Monmouth, NJ 07703
3	Commander ERADCOM Technical Library ATTN: DELSD-L DELEW-E, W. S. McAfee DELSD-EI, J. Roma Fort Monmouth, NJ 07703
8	Commander US Army Harry Diamond Labs ATTN: Mr. James Gaul Mr. L. Belliveau Mr. J. Meszaros Mr. J. Gwaltney Mr. F. W. Balicki Mr. Bill Vault Mr. R. J. Bostak Mr. R. K. Warner 2800 Powder Mill Road Adelphi, MD 20783
4	Commander US Army Harry Diamond Labs ATTN: DELHD-TA-L AMXDO-TI/002 AMXDO-NP DELHD-RBA/J. Rosado 2800 Powder Mill Road Adelphi, MD 20783
1	Commander US Army Infantry School ATTN: ATSH-CD-CSO-OR Fort Benning, GA 31905
1	Commander, U.S. Army Missile Command Research, Development & Engineering Center, ATTN: AMSMI-RD Redstone Arsenal, AL 35898
1	Commander, U.S. Army Missile & Space Intelligence Center ATTN AIAMS-YDL Redstone Arsenal, AL 35898-5500
1	Commander US Army Missile Command ATTN: Technical Library Redstone Arsenal, AL 35898
3	Commander US Army Natick Research and Development Command ATTN: AMDNA-DT Dr. D. Sieling AMXNE-UE/A. Johnson W. Crenshaw Natick, MA 01760
1	Commander US Army Tank Automotive Command ATTN: AMSTA-TSL Warren, MI 48090
1	Commander US Army Foreign Science and Technology Center ATTN: Rsch & Cncepts Br 220 7th Street , NE Charlottesville, VA 22901
1	Commander US Army Logistical Management Center ATTN: ATCL-SCA Mr. Robert Cameron Fort Lee, VA 23801

DISTRIBUTION LIST

No. of Copies	Organization
3	Commander US Army Materials and Mechanics Research Center ATTN: Technical Library AMXMR-ER, Joe Prifti Eugene de Luca Watertown, MA 02172
1	Commander US Army Research Office P.O. Box 12211 Research Triangle Park NC 27709
4	Commander US Army Nuclear and Chemical Agency ATTN: ACTA-NAW MONA-WE Technical Library MAJ Uecke 7500 Backlick Rd, Bldg. 2073 Springfield, VA 22150
1	Commander US Army TRADOC ATTN: ATCD-SA Fort Monroe, VA 23651
2	Director US Army TRADOC Systems Analysis Activity ATTN: LTC John Hesse ATAA-SL, Tech Lib White Sands Missile Range NM 8802
1	Commander HQ, USACAC & FT LVN ATTN: ATCA-CO, Mr. L. C. Pleger Fort Leavenworth, KS 66027-5080
1	Commandant Interservice Nuclear Weapons School ATTN: Technical Library Kirtland AFB, NM 87117
1	Chief of Naval Material ATTN: MAT 0323 Department of the Navy Arlington, VA 22217
2	Chief of Naval Operations ATTN: OP-03EG OP-985F Department of the Navy Washington, DC 20350
1	Chief of Naval Research ATTN: N. Perrone Department of the Navy Washington, DC 20360
1	Director Strategic Systems Projects Ofc ATTN: NSP-43, Tech Library Department of the Navy Washington, DC 20360
1	Commander Naval Electronic Systems Com ATTN: PME 117-21A Washington, DC 20360
1	Commander Naval Facilities Engineering Command ATTN: Technical Library Washington, DC 20360
1	Commander Naval Sea Systems Command ATTN: ORD-91313, Library Department of the Navy Washington, DC 20362

DISTRIBUTION LIST

No. of Copies	Organization
3	Officer-in-Charge (Code L31) Civil Engineering Laboratory Naval Constr Btn Center ATTN: Stan Takahashi R. J. Odello Technical Library Port Hueneme, CA 93041
1	Commander David W. Taylor Naval Ship Research & Development Ctr ATTN: Lib Div, Code 522 Bethesda, MD 20084
1	Commander Naval Surface Weapons Center ATTN: DX-21, Library Br. Dahlgren, VA 22448
2	Commander Naval Surface Weapons Center ATTN: Code WA501/Navy Nuclear Programs Office Code WX21/Tech Library Silver Spring, MD 20910
1	Commander Naval Weapons Center ATTN: Code 533, Tech Lib China Lake, CA 93555
1	Commander Naval Weapons Evaluation Fac ATTN: Document Control Kirtland Air Force Base Albuquerque, NM 87117
1	Commander Naval Research Laboratory ATTN: Code 2027, Tech Lib Washington, DC 20375
1	Superintendent Naval Postgraduate School ATTN: Code 2124, Technical Reports Library Monterey, CA 93940
1	AFSC (Tech Lib) Andrews Air Force Base Washington DC 20331
1	ADTC (Tech Lib) Eglin AFB, FL 32542
1	AFATL (DLYV) Eglin AFB, FL 32542
1	RADC (EMTLD/Docu Libray) Griffiss AFB, NY 13340
1	AFWL/NTES (R. Henny) Kirtland AFB, NM 87117
1	AFWL/NTE, CPT J. Clifford Kirtland AFB, NM 87117
1	AFWL/SUL Kirtland AFB, NM 87117
1	Commander-in-Chief Strategic Air Command ATTN: NRI-STINFO Lib Offutt AFB, NB 68113
1	AFIT (Lib Bldg. 640, Area B) Wright-Patterson AFB Ohio 45433
1	FTD (TD/BTA/Lib) Wright-Patterson AFB Ohio 45433
1	Director Lawrence Livermore Lab. ATTN: Tech Info Dept L-3 P.O. Box 808 Livermore, CA 94550
2	Director Los Alamos National Lab. ATTN: Doc Control for Rpts Lib R. A. Gentry P.O. Box 1663 Los Alamos, NM 87544

DISTRIBUTION LIST

No. of Copies	Organization
2	Director Sandia Laboratories ATTN: Doc Control for 3141 Sandia Rpt Collection L. J. Vortman P.O. Box 5800 Albuquerque, NM 87115
1	Director Sandia Laboratories Livermore Laboratory ATTN: Doc Control for Tech Lib P.O. Box 969 Livermore, CA 94550
1	Director National Aeronautics and Space Administration Scientific & Tech Info Fac P.O. Box 8757 Baltimore/Washington International Airport MD 21240
2	ADINA Engineering Inc. ATTN: Dr. Anil Chaudhary Dr. K.J. Bathe 71 Elkton Avenue Watertown, MA. 02172
1	Aerospace Corporation ATTN: Tech Info Services P.O. Box 92957 Los Angeles, CA 90009
1	Agbabian Associates ATTN: M. Agbabian 250 North Nash Street El Segundo, CA 90245
1	The BDM Corporation ATTN: Richard Hensley P.O. Box 9274 Albuquerque International Albuquerque, NM 87119
1	The Boeing Company ATTN: Aerospace library P.O. Box 3707 Seattle, WA 98124
2	California Research and Technology ATTN: M. Rosenblatt F. Sauer 20943 Devonshire Street Chatsworth, CA 91311
1	Goodyear Aerospace Corp ATTN: R. M. Brown, Bldg 1 Shelter Engineering Litchfield Park, AZ 85340
5	Kaman AviDyne ATTN: Dr. N.P. Hobbs (4 cys) Mr. S. Criscione 83 Second Avenue Northwest Industrial Park Burlington, MA 01803
3	Kaman Sciences Corporation ATTN: Library P. A. Ellis F. H. Shelton 1500 Garden of the Gods Road Colorado Springs, CO 80907
1	Kaman-TEMPO ATTN: DASIAC P.O. Drawer QQ Santa Barbara, CA 93102
1	Kaman-TEMPO ATTN: E. Bryant, Suite UL-1 715 Shamrock Road Bel Air, MD 21014
1	Lockheed Missiles & Space Co. ATTN: J. J. Murphy, Dept. 81-11, Bldg. 154 P.O. Box 504 Sunnyvale, CA 94088

DISTRIBUTION LIST

No. of Copies	Organization
1	Martin Marietta Aerospace Orlando Division ATTN: G. Fotieo P.O. Box 5837 Orlando, FL 32805
2	McDonnell Douglas Astronautics Corporation ATTN: Robert W. Halprin Dr. P. Lewis 5301 Bolsa Avenue Huntington Beach, CA 92647
1	The Mitre Corporation ATTN: Library P.O. Box 208 Bedford, MA 01730
1	New Mexico Engineering Research Institute (CERF) ATTN: J. Leigh P.O. Box 25 UNM Albuquerque, NM 87131
1	Pacific Sierra Research Corp ATTN: Dr. Harold Brode 1456 Cloverfield Boulevard Santa Monica, CA 90404
2	Physics International Corp ATTN: Technical Library Mr. Fred Sauer 2700 Merced Street San Leandro, CA 94577
1	Radkowski Associates ATTN: Peter R. Radkowski P.O. Box 5474 Riverside, CA 92517
2	R&D Associates ATTN: Technical Library Allan Kuhl P.O. Box 9695 Marina del Rey, CA 90291
1	R&D Associates ATTN: G.P. Ganong P.O. Box 9330 Albuquerque, NM. 87119
1	RCA Government Communications Systems 13-5-2 Front & Cooper Streets Camden, NJ 08102
2	Science Applications, Inc. ATTN: Burton S. Chambers John Cockayne P.O. BOX 1303 1710 Goodridge Drive McLean, VA 22102
1	Science Applications, Inc. ATTN: Technical Library P.O. Box 2351 La Jolla, CA 92038
1	Systems, Science and Software ATTN: C. E. Needham P.O. Box 8243 Albuquerque, NM 87198
3	Systems, Science and Software ATTN: Technical Library R. Duff K. Pyatt P.O. Box 1620 La Jolla, CA 92037
1	TRW Electronics & Defense ATTN: Benjamin Sussholtz One Space Park, 134/9048 Redondo Beach, CA 92078
2	Union Carbide Corporation Holifield National Laboratory ATTN: Doc Control for Tech Lib Civil Defense Research Proj PO Box X Oak Ridge, TN 37830

DISTRIBUTION LIST

No. of Copies	Organization
1	Weidlinger Assoc. Consulting Engineers ATTN: M. L. Baron 110 East 59th Street New York, NY 10022
1	Battelle Memorial Institute ATTN: Technical Library 505 King Avenue Columbus, OH 43201
1	California Inst of Tech ATTN: T. J. Ahrens 1201 E. California Blvd. Pasadena, CA 91109
2	Denver Research Institute University of Denver ATTN: Mr. J. Wisotski Technical Library PO Box 10127 Denver, CO 80210
1	IIT Research Institute ATTN: Milton R. Johnson 10 West 35th Street Chicago, IL 60616
1	TRW Ballistic Missile Division ATTN: H. Korman, Mail Station 526/614 P.O. Box 1310 San Bernadino, CA 92402
1	H. Jerry Carpenter Carpenter Research Corporation Suite 424, 904 Silver Spur Rd Rolling Hills Estates CA 90274
1	J. D. Haltiwanger Consulting Services B106a Civil Engineering Bldg. 208 N. Romine Street Urbana, IL 61801
1	Massachusetts Institute of Technology Aeroelastic and Structures Research Laboratory ATTN: Dr. E. A. Witmer Cambridge, MA 02139
2	Massachusetts Institute of Technology Mechanical Engineering Dept. ATTN: Prof. K. J. Bathe Dr. Eduardo N. Dvorkin Cambridge, MA 02139
2	Southwest Research Institute ATTN: Dr. W. E. Baker A. B. Wenzel 8500 Culebra Road San Antonio, TX 78228
1	SRI International ATTN: Dr. G. R. Abrahamson 333 Ravenswood Avenue Menlo Park, CA 94025
1	Stanford University ATTN: Dr. D. Bershader Durand Laboratory Stanford, CA 94305
1	Washington State University Physics Department ATTN: G. R. Fowles Pullman, VA 99164

Aberdeen Proving Ground

Dir, USAMSAA
ATTN: AMXSY-D
AMXSY-MP, H. Cohen
Cdr, USATECOM
ATTN: AMSTE-TO-F
Cdr, CRDC, AMCCOM,
ATTN: SMCCR-RSP-A
SMCCR-MU
SMCCR-SPS-IL